

1

Title

2

## **Spike burst–pause dynamics of Purkinje cells regulate sensorimotor adaptation**

4

Abbreviated title

5

## **Burst-pause Purkinje dynamics regulate motor adaptation**

7

Niceto R. Luque<sup>1</sup>, Francisco Náveros<sup>2</sup>, Richard R. Carrillo<sup>2</sup>, Eduardo Ros<sup>2¶</sup> and  
8 Angelo Arleo<sup>1¶</sup>

9

10 <sup>1</sup> Sorbonne Universités, UPMC Université Paris 06, INSERM, CNRS, Institut de la  
11 Vision, Paris, France

12 <sup>2</sup> Department of Computer Architecture and Technology, CITIC-University of Granada,  
13 Granada, Spain

14 \* Corresponding authors: Niceto R. Luque, and Angelo Arleo

15 E-mail: [nluque@ugr.es](mailto:nluque@ugr.es), [angelo.arleo@inserm.fr](mailto:angelo.arleo@inserm.fr)

16 ¶ AA and ER are Joint Senior Authors

17

18

19

20

21 **Abstract**

22 Cerebellar Purkinje cells mediate accurate eye movement coordination. However, it  
23 remains unclear how oculomotor adaptation depends on the interplay between the  
24 characteristic Purkinje cell response patterns, namely tonic, bursting, and spike pauses.  
25 Here, a spiking cerebellar model assesses the role of Purkinje cell firing patterns in  
26 vestibular ocular reflex (VOR) adaptation. The model captures the cerebellar  
27 microcircuit properties and it incorporates spike-based synaptic plasticity at multiple  
28 cerebellar sites. A detailed Purkinje cell model reproduces the three spike-firing patterns  
29 that are shown to regulate the cerebellar output. Our results suggest that pauses following  
30 Purkinje complex spikes (bursts) encode transient disinhibition of targeted medial  
31 vestibular nuclei, critically gating the vestibular signals conveyed by mossy fibres. This  
32 gating mechanism accounts for early and coarse VOR acquisition, prior to the late reflex  
33 consolidation. In addition, properly timed and sized Purkinje cell bursts allow the ratio  
34 between long-term depression and potentiation (LTD/LTP) to be finely shaped at mossy  
35 fibre-medial vestibular nuclei synapses, which optimises VOR consolidation. Tonic  
36 Purkinje cell firing maintains the consolidated VOR through time. Importantly, pauses  
37 are crucial to facilitate VOR phase-reversal learning, by reshaping previously learnt  
38 synaptic weight distributions. Altogether, these results predict that Purkinje spike burst-  
39 pause dynamics are instrumental to VOR learning and reversal adaptation.

40

41 **Author Summary**

42 Cerebellar Purkinje cells regulate accurate eye movement coordination. However, it  
43 remains unclear how cerebellar-dependent oculomotor adaptation depends on the  
44 interplay between Purkinje cell characteristic response patterns: tonic, high-frequency  
45 bursting, and post-complex spike pauses. We explore the role of Purkinje spike burst-  
46 pause dynamics in VOR adaptation. A biophysical model of Purkinje cell is at the core  
47 of a spiking network model, which captures the cerebellar microcircuit properties and  
48 incorporates spike-based synaptic plasticity mechanisms at different cerebellar sites. We  
49 show that Purkinje spike burst-pause dynamics are critical for (1) gating the vestibular-  
50 motor response association during VOR acquisition; (2) mediating the LTD/LTP  
51 balance for VOR consolidation; (3) reshaping synaptic efficacy distributions for VOR  
52 phase-reversal adaptation; (4) explaining the reversal VOR gain discontinuities during  
53 sleeping.

54

55 **Introduction**

56 The cerebellum controls fine motor coordination including online adjustments of eye  
57 movements [1]. Within the cerebellar cortex, the inhibitory projections of Purkinje cells  
58 to medial vestibular nuclei (MVN) mediate the acquisition of accurate oculomotor  
59 control [2, 3]. Here, we consider the role of cerebellar Purkinje cells in the adaptation of  
60 the vestibular ocular reflex (VOR), which generates rapid contralateral eye movements  
61 that maintain images in the fovea during head rotations (Fig 1A). The VOR is crucial to  
62 preserve clear vision (e.g., whilst reading) and maintain balance by stabilising gaze  
63 during head movements. The VOR is mediated by the three-neuron reflex arc comprised  
64 of connections from the vestibular organ via the medial vestibular nuclei (MVN) to the  
65 eye motor neurons [3-5]. VOR control is purely feed-forward [6] and it relies on several  
66 cerebellar-dependent adaptive mechanisms driven by sensory errors (Fig 1B). Because  
67 of its dependence upon cerebellar adaptation, VOR has become one of the most  
68 intensively used paradigms to assess cerebellar learning [6]. However, very few studies  
69 have focused on the relation between the characteristics spike response patterns of  
70 Purkinje cells and VOR adaptation, which is the main focus of this study.

71

72 **Figure 1. Vestibular Ocular Reflex (VOR) and cerebellar control loop. (A) Horizontal**  
73 **VOR (h-VOR) protocols compare head rotational movements (input) against the induced**  
74 **contralateral eye movements (output) via two measurements: the VOR gain, i.e. the ratio**  
75 **between eye and head speeds ( $E_v$  and  $H_v$ , respectively); and the VOR phase, i.e. the**  
76 **temporal lag between eye and head velocity signals. (B) Cerebellar feed-forward control**  
77 **system comparing a known reference (head velocity or input variable) to the actual**  
78 **output (eye velocity) to quantify an error signal driving adaptation. The cerebellum**

79 *compensates for the difference between actual eye (represented as an inverter logic gate*  
80 *in this scheme) and head velocity profiles. The head velocity consists of a 1 Hz sinusoidal*  
81 *function iteratively presented to the cerebellar model, mimicking the sinusoidal*  
82 *frequency of the head rotation in experimental protocols [7]. (C) Schematic*  
83 *representation of the main neural layers, cells, connections and plasticity sites*  
84 *considered in the cerebellar model. Mossy fibres (MFs) convey the sensory signals from*  
85 *the vestibular organ and they provide the input to the cerebellar network. MFs project*  
86 *sensorimotor information onto granular cells (GCs) and medial vestibular nuclei*  
87 *(MVN). GCs, in turn, project onto Purkinje cells through parallel fibres (PFs). Purkinje*  
88 *cells also receive excitatory inputs from the climbing fibres (CFs). CFs deliver the error*  
89 *signals encoding instructive terms that drive motor control learning. Purkinje cells*  
90 *integrate CF and PF inputs, thus transmitting the difference between head and eye*  
91 *movements. Finally, MVN are inhibited by Purkinje cells and provide the main*  
92 *cerebellar output. The cerebellar model implements different spike timing dependent*  
93 *plasticity mechanisms at multiple sites: PF-Purkinje cell, MF-MVN, and Purkinje cell-*  
94 *MVN synapses.*

95

96        Purkinje cells provide the major output of the cerebellum through MVN. Purkinje  
97    cells receive two main excitatory (glutamatergic) afferent currents (Fig 1C). The first  
98    excitatory input originates from the parallel fibres (PFs), i.e. the axons of the granule  
99    cells (GCs). The second comes from the climbing fibres (CFs), i.e. the projections of the  
100   inferior olive (IO) cells. These excitatory inputs drive Purkinje cell simple or complex  
101   spike patterns, respectively [8, 9]. Simple spikes of Purkinje cells are elicited tonically  
102   at high frequencies [10, 11]. Complex spikes consist of a fast initial large-amplitude  
103   spike followed by a high-frequency burst [12]. This burst is made of several slower

104 spikelets of smaller amplitude separated from one another by 2-3 ms [12-14]. Complex  
105 spikes are caused by the activation of a single IO neuron that produces a large electrical  
106 event in the soma of the post-synaptic Purkinje cell. This electrical event generates  
107 calcium-mediated action potentials in the Purkinje cell dendrites that, in turn, shape the  
108 complex spike. Simple spike activity is, in fact, mostly suppressed during complex  
109 spiking [14]. After each CF-evoked burst, a spike pause prevents Purkinje cells from  
110 either resuming their tonic or bursting firing for a period that depends on the length of  
111 the complex spike [15]. The CF-evoked spike burst-pause sequences of Purkinje cell  
112 responses critically regulate the inhibitory (GABAergic) drive of MVN synapses, which  
113 determines the cerebellar output during sensorimotor adaptation. Therefore,  
114 understanding the dynamics of the characteristic Purkinje cell spike patterns is relevant  
115 to linking cerebellar cell properties to cerebellar-dependent behavioural adaptation.  
116 Recent studies have paved the road in gaining knowledge on the behavioural implication  
117 of Purkinje cell spike modes [2, 14, 16]. In particular, Herzfeld and colleagues have  
118 demonstrated that the cerebellum encodes real-time motion of the eye through the  
119 organisation of Purkinje cells into clusters that share similar CF projections from the IO  
120 [2]. The combined activity of bursting and silent Purkinje cell populations can predict  
121 both the actual speed and direction of rapid accurate eye movements (saccades).  
122 However, these studies have not assessed the interplay between the different Purkinje  
123 cell spike patterns and the plasticity mechanisms at stake at MVN synapses in shaping  
124 sensorimotor adaptation. MVN neurons, in addition to receiving the inhibitory inputs  
125 from Purkinje cells, are also innervated by the excitatory afferents from the mossy fibres  
126 (MFs), which convey vestibular signals about head movements (Fig 1C). This vestibular  
127 information also converges onto Purkinje cells through the mossy fibre-granule cell-  
128 parallel fibre pathway (MF-GC-PF; Fig 1C). Therefore, the characteristics firing patterns

129 of Purkinje cells are likely to play a key role in driving the associative plasticity  
130 mechanisms operating at MF-MVN excitatory synapses [17-19] and at Purkinje cells-  
131 MVN inhibitory synapses [20-23]. The CF-evoked spike burst-pause sequences of  
132 Purkinje cells depend indeed upon the activation of CFs, which are assumed to convey  
133 a ‘teaching’ signal encoding sensory error information [6, 14, 24]. Therefore, the  
134 properties of the CF-evoked spike burst-pause patterns (e.g., the relative duration of the  
135 bursts versus the pauses) reflect sensory error related information [14, 16]. The  
136 activation of CFs is critical for inducing different forms of plasticity at PF-Purkinje cell  
137 synapses and, indirectly, at Purkinje cell-MVN synapses [25, 26]. Importantly, plasticity  
138 at MF-MVN synapses also seems to be dependent on Purkinje cell signals [27-29],  
139 generated through the MF-GC-PF pathway and through CF activation. Some  
140 computational studies have proposed that plasticity mechanisms at MF-MVN and  
141 Purkinje cell-MVN synapses are key factors in determining cerebellar adaptive gain  
142 control [27, 28, 30]. These models support the hypothesis of a two-state cerebellar  
143 adaptation process [31, 32], with a fast adaptive phase mediated by the cerebellar cortex  
144 (involving plasticity at Purkinje cell synapses) and a slow adaptive process occurring in  
145 deeper structures, involving plasticity at MVN synapses [29, 31-35]. However, these  
146 computational studies do not account for the interaction between the different spiking  
147 modes of Purkinje cells (in particular CF-evoked spike burst-pause dynamics) and the  
148 distributed plasticity mechanisms underpinning cerebellar adaptive control [30].

149 The spiking cerebellar model presented here addresses these issues within a VOR  
150 adaptation framework (Figs 1A,B). We simulate horizontal VOR (h-VOR) experiments  
151 with mice undertaking sinusoidal (~1 Hz) whole body rotations in the dark [36]. The  
152 model incorporates the main anatomo-functional properties of the cerebellar

153 microcircuit, with synaptic plasticity mechanisms at multiple cerebellar sites (Fig 1C;  
154 see Materials & Methods).

155 **Results**

156 ***Spike burst–pause properties of model Purkinje cell responses***

157 The detailed Purkinje cell model reproduces the characteristic response patterns  
158 observed experimentally: tonic simple spiking (20-200 Hz), complex spiking (bursts  
159 with high-frequency spikelet components up to 600 Hz), and post-complex spike pauses  
160 (Fig 2A). In the model, CF discharges trigger transitions between the Purkinje cell  $\text{Na}^+$   
161 spike output, CF-evoked bursts, and post-complex spike pauses. As evidenced in [37],  
162 in *in-vitro* slice preparations at normal physiological conditions, 70% of Purkinje cells  
163 spontaneously express a trimodal oscillation: a  $\text{Na}^+$  tonic spike phase, a  $\text{Ca}-\text{Na}^+$  bursting  
164 phase, and a hyperpolarised quiescent phase. On the other hand, Purkinje cells also show  
165 spontaneous firing consisting of a tonic  $\text{Na}^+$  spike output without  $\text{Ca}-\text{Na}^+$  bursts [37-  
166 39]. McKay et al. [37] report Purkinje cell recordings exhibiting a tonic  $\text{Na}^+$  phase  
167 sequence followed by CF-evoked bursts (via complex spikes) and the subsequent pause  
168 (Fig 2A). The frequency of Purkinje cell  $\text{Na}^+$  spike output decreases with no correlation  
169 with the intervals between CF discharges. The model mimics this behaviour under  
170 similar CF discharge conditions (Fig 2B).

171 The duration of model post-complex spike pauses increases linearly with burst  
172 duration (Fig 2C;  $R^2=0.82$ ,  $p<0.0001$ ). To assess the relation between burst and pause  
173 duration, the depolarisation current injected through PF was maintained constant whilst  
174 progressively increasing the intensity of CF stimulation. Only inter-spike intervals (ISIs)  
175 immediately following complex spikes were considered for this analysis. The model  
176 replicates the linear relation between spike pause duration and *pre-complex* spike ISI

177 duration observed through electrophysiological recordings [40] (Fig 2D;  $R^2=0.9879$ ;  
178 p<0.0001). This relation was measured by maintaining the CF stimulation constant  
179 whilst incrementally increasing the amplitude of the PF input current. The probability  
180 distribution of *post-complex* spike ISIs is also consistent with experimental data [40]  
181 (Fig 2E). The kurtosis ('peakedness') of the ISI distribution is 4.24, which is in the range  
182 of kurtosis values measured after tetanisation of mouse Purkinje cells [40]. Finally,  
183 model *post-complex* spike ISI values are skewed rightward (positive skewness value of  
184 0.6463), consistently with the asymmetric distribution shape observed experimentally  
185 [40].

186

187 **Figure 2. Spike burst–pause properties of model Purkinje cell responses. (A)** Simulated  
188 (left) and electrophysiological (right) recordings of Purkinje cell spike outputs in  
189 response to CF spike excitatory postsynaptic potentials occurring at physiological  
190 frequencies (arrows) (data from [37]). CF discharges trigger transitions between  
191 Purkinje cell  $Na^+$  spike output and CF-evoked bursts and pauses via complex spikes.  
192 Here, the Purkinje cell model was run on the EDLUT simulator (see Methods). **(B)**  
193 Simulated (left) and experimental (right) Purkinje cell tonic spike frequency during CF  
194 discharges aligned with spike-grams in A (data from [37]). N=10 Purkinje cells were  
195 simulated to compute the tonic spike frequency. **(C)** In the model, CF signals modulate  
196 both the burst size (i.e., the number of spikes within the burst) and the duration of post-  
197 complex spike pauses, which are linearly correlated. Here, the Purkinje cell model was  
198 run on the Neuron simulator (see Methods). **(D)** Relation between pause duration and  
199 pre-complex spike (pre-CS) inter spike intervals (ISIs) when increasing the amplitude  
200 of the injected current: model data (red circles, n=1000) vs. experimental data [40]  
201 (grey to black dots). Grey-to-black lines represent individual cells (n=10). The blue

202 *dashed line is the linear regression curve fitting model data. The model captures the*  
203 *linear relation between spike pause duration and pre-complex spike ISI duration*  
204 *observed electrophysiologically [40]. (E) Distribution of ISI values following the*  
205 *complex spike (post-CS). The ISI duration is normalised to pre-CS ISI values. The*  
206 *Kurtosis for the distribution of post-CS ISI values is 4.24. The skewness is positive*  
207 *(0.6463), thus indicating an asymmetric post-CS ISI distribution. Kurtosis and skewness*  
208 *values were consistent with Purkinje cell data [40].*

209

## 210 **Role of cerebellar Purkinje spike burst-pause dynamics in VOR adaptation**

211 We assessed h-VOR adaptation by simulating a 1 Hz horizontal head rotation to be  
212 compensated by contralateral eye movements (Fig 1A). First, we tested the role of  
213 Purkinje spike burst-pause dynamics in the absence of cerebellar learning, i.e. by  
214 blocking synaptic plasticity across all model projections (i.e., MF-MVN, PF-Purkinje  
215 cell, Purkinje cell-MVN). Synaptic weights were initialised randomly and equally within  
216 each projection set. The CF input driving Purkinje cells was taken as to signal large  
217 retina slips, which generated sequences of complex spikes made of 4 to 6 burst spikelets  
218 [14] (Fig 3A, top). The elicited Purkinje spike burst-pause sequences shaped the  
219 temporal disinhibition of targeted VN neurons, allowing the incoming input from MFs  
220 to drive MVN responses (Fig 3A, middle). This facilitated a coarse baseline eye motion  
221 (Fig 3A, bottom). Blocking complex spiking in the Purkinje cell model (through the  
222 blockade of muscarinic voltage-dependent channels, see Methods) prevented MF  
223 activity from eliciting any baseline MVN compensatory output (Fig 3B). These results  
224 suggest that the gating mechanism mediated by Purkinje spike burst-pause sequences,  
225 which encode transient disinhibition of MVN neurons, is useful for early and coarse  
226 VOR, prior to the adaptive consolidation of the reflex through cerebellar learning.

227

228 **Figure 3. Purkinje post-complex spike pauses act as a gating mechanism for early**  
229 **coarse VOR in the absence of cerebellar adaptation.** Only half of h-VOR cycle is  
230 represented. Two equal cerebellar network configurations except for the Purkinje cell  
231 dynamics were compared under equal stimulation. **(A)** The first model accounts for CF-  
232 evoked Purkinje spike burst-pause dynamics. CF stimulation generates complex spikes  
233 and subsequent post-complex spike pauses. The latter allows MFs to drive directly the  
234 immediate activation of MVN, which facilitates an early but rough eye movement  
235 compensation for head velocity. **(B)** The second model only exhibits Purkinje tonic firing  
236 (i.e., complex spiking is blocked through the blockade of muscarinic voltage-dependent  
237 channels, see Methods), which prevents MFs from eliciting any baseline MVN  
238 compensatory output. See S3-1 and S3-2 Figs for a sensitivity analysis of parameters  
239 regulating the LTD/LTP balance at PF-Purkinje cell and MF-MVN synapses. See also  
240 S3-3 Fig for the same parameter sensitivity analysis in the absence of Purkinje spike  
241 burst-pause dynamics.

242

243 We then activated the LTD/LTP plasticity mechanisms at MF-MVN, PF-Purkinje  
244 cell, and Purkinje cell-MVN synapses (see Materials & Methods). During 10000 s, the  
245 model faced a 1 Hz horizontal head rotation, and cerebellar h-VOR learning took place  
246 to generate compensatory contralateral eye movements. A sensitivity analysis identified  
247 the critical LTD/LTP balance at MF-MVN and PF-Purkinje cell synapses in order to  
248 achieve VOR adaptation (in terms of both gain and phase). This analysis predicts a very  
249 narrow range of values for which LTP slightly exceeding LTD at MF-MVN synapses  
250 ensures learning stability through time. By contrast, PF-Purkinje cell synapses admitted  
251 a significantly broader range for the LTD/LTP ratio (S3-1 and S3-2 Figs). The same

252 parameter sensitivity analysis for the cerebellar model with no bursting and pause  
253 dynamics shows a much wider range of values for the LTD/LTP balance at both PF-  
254 Purkinje cell and MF-MVN synapses (S3-3 Fig).

255 A comparison of VOR adaptation accuracy in the presence vs. absence of CF-  
256 evoked Purkinje spike burst-pause dynamics shows that VOR gain plateaued three times  
257 faster in the presence of Purkinje complex spikes (Fig 4A, left). Also, the VOR gain  
258 converged to [0.8-0.9], which is consistent with experimental recordings in mice [36],  
259 monkeys [41], and humans [42]. Conversely, without Purkinje bursting-pause dynamics  
260 the VOR gain saturated to a value  $>1$  (i.e., over learning) at the end of the adaptation  
261 process. In terms of VOR phase, convergence to  $180^\circ$  (i.e., well synchronised counter-  
262 phase eye movements) was reached after approximately 1000 s under both conditions  
263 (Fig 4A, right).

264 A more accurate VOR gain adaptation in the presence of Purkinje complex spiking  
265 reflected a more selective synaptic modulation across learning (Figs 4B-D). In particular,  
266 Purkinje spike burst-pause dynamics facilitated a sparser weight distribution at MF-  
267 MVN synapses (Fig 4B), which ultimately shaped VOR adaptation [18]. Indeed,  
268 Purkinje burst sizes reflected the sensed errors [14], thus regulating the inhibitory action  
269 of Purkinje cells on MVN, and inducing error-dependent LTD at MF-MVN synapses  
270 (see Materials & Methods). On the other hand, post-complex spike pauses (disinhibiting  
271 MVN) induced error-dependent LTP at MF-MVN synapses (the larger the error, the  
272 larger the burst size, and the wider the post-complex spike pause, Fig 2B). At the  
273 beginning of VOR adaptation, the error was larger, and so were the burst and pause  
274 durations. Because the durations of pauses remained always larger than bursts (Fig 2B),  
275 LTP dominated over LTD at MF-MVN synapses, increasing the learning rate. Therefore,  
276 the spike burst-pause dynamics enhanced the precision of cerebellar adaptation at MVN

277 cells, by (i) recruiting the strictly necessary MF-MVN projections (i.e., higher kurtosis  
278 value of the synaptic weight distribution, Fig 4B), (ii) making a better use of the synaptic  
279 range of selected projections (larger standard deviations with lower overall gains; Fig  
280 4C), and the rate by (iii) varying synaptic weights selectively (lower averaged synaptic  
281 weight variations; Fig 4D).

282

283 **Figure 4. Role of Purkinje spike burst-pause dynamics in VOR cerebellar adaptation.**  
284 **(A)** *VOR gain and phase adaptation with (purple curve) and without (green curve) CF-  
285 evoked Purkinje spike burst-pause dynamics. VOR cerebellar adaptation starts with zero  
286 gain owing to the initial synaptic weights at PF and MVN afferents (Table 5). Purkinje  
287 spike burst-pause dynamics provides better VOR gain adaptation (in terms of both rate  
288 and precision) converging to values within [0.8-0.9], which is consistent with  
289 experimental data [36, 41, 42]. **(B)** Purkinje complex spiking allows a sparser weight  
290 distribution (with higher Kurtosis) to be learnt at MF-MVN synapses, with significantly  
291 lesser MF afferents needed for learning consolidation. **(C)** The model endowed with  
292 Purkinje complex spiking updates less MF afferents during learning consolidation but  
293 their synaptic range is fully exploited. **(D)** The averaged synaptic weight variations are  
294 more selective during the adaptive process in the presence of Purkinje spike burst-pause  
295 dynamics, yet the standard deviation remains equal.*

296

297 **Purkinje spike burst-pause dynamics facilitates VOR phase-reversal learning**

298 Phase-reversal VOR is induced when a visual stimulus is given simultaneously in phase  
299 to the vestibular stimulation but at greater amplitude (10% more) [25]. This creates a  
300 mismatch between visual and vestibular stimulation making retinal slips to reverse

301 direction[43]. Cerebellar learning is deeply affected by VOR phase reversal since the  
302 synaptic weight distribution at both PF-Purkinje cell and MF-MVN synapses must be  
303 reversed. Here, we first simulated an h-VOR adaptation protocol (1 Hz) during 10000 s  
304 (as before). Then, h-VOR phase reversal took place during the next 12000 s. Finally, the  
305 normal h-VOR had to be restored during the last 12000 s (Fig 5). Our results suggest  
306 that Purkinje spike burst-pause dynamics were instrumental to phase-reversal VOR gain  
307 adaptation (Fig 5A), allowing for fast VOR learning reversibility consistently with  
308 experimental recordings [3] (Fig 5B). Conversely, the absence of Purkinje complex  
309 spiking led to impaired VOR phase-reversal learning with significant interference (Figs  
310 5A,B). The two models (i.e., with and without Purkinje complex spiking) behaved  
311 similarly in terms of VOR phase adaptation during the same reversal learning protocol  
312 (S5-1 Fig).

313

314 **Figure 5. Purkinje spike burst-pause dynamics facilitates VOR phase-reversal**  
315 **learning. (A)** VOR gain adaptation with (red curve) and without (green curve) Purkinje  
316 spike burst-pause dynamics during: VOR adaptation (first 10000 s), phase-reversal  
317 learning (subsequent 12000 s), and normal VOR restoration (remaining 12000 s). **(B)**  
318 Purkinje spike burst-pause dynamics provides fast learning reversibility, consistently  
319 with experimental recordings [3]. By contrast, phase-reversal VOR learning is impaired  
320 in the absence of Purkinje complex spiking. See S5-1 Fig for the time course of VOR  
321 phase-reversal learning.

322

323 VOR phase-reversal learning demanded first the reduction of the VOR gain, which  
324 can be regarded as a ‘forgetting phase’ (Fig 5B, days 1&2). Then, a ‘synchronisation

325 phase' took place with a reverse adaptive action that gradually increased the VOR gain  
326 (Fig 5B, days 3&4). During the forgetting phase, LTD dominated over LTP at MF-MVN  
327 synapses (Purkinje burst sizes were maximal), thus erasing the memorised weight  
328 patterns. During the synchronisation phase, Purkinje post-complex spike pauses led to a  
329 dominant LTP at MF-MVN synapses, reversing the learnt configuration. The interplay  
330 between bursts and post-complex spike pauses allowed synaptic adaptation at MF-MVN  
331 projections to be highly selective, which resulted in a sparser weight distribution as  
332 compared to the case without Purkinje complex spiking (Fig 6A). Therefore, VOR  
333 reverse learning required the adjustment of fewer MF-MVN synapses, thus facilitating  
334 the eye counteraction of the head velocity movement (S6-1 Fig), and the weight  
335 distribution was reshaped more efficiently with negligible interferences from the  
336 previously learnt patterns (Figs 6B, C).

337

338 **Figure 6. Evolution of synaptic weight distributions during VOR phase-reversal**  
339 **learning. (A)** Only the sparser and more selective distribution of MF-MVN synaptic  
340 weights resulting from the interplay between bursts and post-complex spike pauses  
341 facilitates an efficient reshaping of the learnt patterns **(B)**, allowing phase-reversal  
342 learning to be achieved **(C)**.

343

344 **LTP blockades (by dominant LTD) during REMs explain reversal VOR gain**  
345 **discontinuities between training sessions**

346 VOR phase-reversal learning can take place across several days [3] (Fig 5). Dark periods  
347 in-between training sessions cause reversal VOR gain discontinuities (Fig 7). This  
348 phenomenon has been assumed to result from the decaying of synaptic weights back to

349 their initial values during sleep [3]. However, the mechanisms underlying this decaying  
350 process remain unknown. We explored possible cerebellar LTD/LTP balance  
351 modulation scenarios occurring during sleep as a consequence of changes in cerebellar  
352 activity. During rapid eye movement sleep (REMs), the mean firing activity of Purkinje  
353 cells shows increased tonic firing and decreased bursting in both frequency and size [44].  
354 The CF average activity during REMs remains constant at a low frequency regime,  
355 showing a tendency in many IO neurons to diminish their overall frequency [45]. The  
356 activation of MFs varies during REMs, unrelatedly to any apparent behavioural changes,  
357 up to 60 MF/s on average [45].

358 We modelled Purkinje cell, CF and MF activities during REMs. CFs were  
359 stochastically activated at 1 Hz [44, 45] following a Poisson distribution (S7-1 Fig). CF  
360 activations were also modulated to generate a large event in the Purkinje soma able to  
361 elicit bursts of 3 spikes on average [44]. MFs were stochastically activated by mimicking  
362 their activity during REMs (with an upper bound firing rate of 8-13 Hz). We tested three  
363 hypotheses, based on different levels of cerebellar activity during 6 REMs stages of 3000  
364 s each (i.e., 18000 s of simulation) between days 1 and 2. In the first scenario, we  
365 considered high levels of MF activity (average firing rate 10 Hz), which led to a  
366 dominance of LTP at both PF-Purkinje cell and MF-MVN synapses during REMs.  
367 Consequently, the cerebellar model kept ‘forgetting’ the memory traces as during the  
368 reversal VOR learning of day 1 (Fig 7, blue curve). In the second scenario, we considered  
369 an average MF activity of 2.5 Hz, which made the LTP driven by vestibular activity to  
370 counterbalance the LTD driven by the CFs. Under this condition, the cerebellar model  
371 consolidated reversal VOR adaptation thus maintaining the synaptic weights at PF-  
372 Purkinje and MF-MVN synapses (Fig 7, green curve). Finally, we considered a low level  
373 of MF activity (average 1 Hz), which made LTD to block the LTP action driven by the

374 vestibular (MF) activity. Under this third scenario, the cerebellar model showed a  
375 consistent tendency for weights at PF-Purkinje and MF-MVN synapses to decay back  
376 towards their initial value (Fig 7, red curve). Therefore, the model predicts that LTP  
377 blockade during REMs stages might underlie the reversal VOR gain discontinuities in-  
378 between training sessions, in agreement with experimental data [3] (Fig 7, black curve).

379

380 **Figure 7. LTP blockades (due to dominant LTD) during REMs explain reversal VOR**  
381 **gain discontinuities between training sessions.** We simulated 6 REMs stages (for a total  
382 of 18000 s of simulation) between day 1 and 2 of VOR phase-reversal learning. High  
383 levels of MF activity (10 Hz) leads to a dominance of LTP at both PF-Purkinje cell and  
384 MF-MVN synapses during REMs. Hence, during REMs the cerebellar model keeps  
385 'forgetting' the memory traces as during day 1 (blue curve). A smaller MF activity (2.5  
386 Hz) leads to a balance of LTP (driven by vestibular activity) and LTD (driven by the  
387 CFs). Thus, the model tends to maintain the synaptic weights learnt during day 1 (orange  
388 curve). A very low MF activity (1 Hz) makes LTD to block LTP at PF-Purkinje and MF-  
389 MVN synapses. Under this third hypothesis, the synaptic weights tend to decay back  
390 towards their initial value (purple curve) in accordance with experimental data [3]. See  
391 S7-1 Fig for the modelled probabilistic Poisson process underpinning CF activation.

392

### 393 **Purkinje complex spike-pause dynamics under stationary VOR conditions**

394 During transient VOR adaptation and phase reversal learning, retina slips were large  
395 causing vigorous CF discharges (up to 10 Hz) to encode the sensed errors. Consequently,  
396 Purkinje cell complex spike-pauses were elicited at high frequency during adaptation  
397 (Fig 8A). As the VOR error decreased, the frequency of CF-evoked Purkinje bursts

398 decayed to ~1 Hz upon completion of adaptation (Fig 8B). Therefore, during post (and  
399 pre) VOR adaptation, model Purkinje tonic  $\text{Na}^+$  spike output dominated and Purkinje  
400 cells tended to fire steadily (similar to spontaneous activity) with only rare complex  
401 spike-pause firing. Under stationary VOR conditions, (i.e., during pre/post VOR  
402 adaptation) model CFs were stochastically activated at ~1 Hz (S7-1 Fig shows the  
403 Poisson-based generative model for the IO firing). Such a CF baseline discharge at ~1  
404 Hz allowed non-supervised LTP to be counterbalanced at PF-Purkinje cell synapses (see  
405 Materials & Methods), thus preserving pre/post cerebellar adaptation.

406 Luebke and Robinson [46] found that directly stimulating CFs at 7 Hz during 30  
407 min after 3 days of VOR adaptation would impair the reflex. Model CFs discharged at  
408 frequencies larger than 1 Hz only to signal retina slips (i.e., during VOR adaptation).  
409 However, a direct (and error independent) high-frequency stochastic stimulation of CFs  
410 would lead to VOR impairment. To illustrate this, we simulated a protocol similar to the  
411 one used by [46]. As expected, the number of CF-evoked Purkinje burst-pauses  
412 increased as the CF frequency was artificially incremented through a 7 Hz direct  
413 stimulation (Fig 8A). Therefore, the VOR gain error tended to increase indicating an  
414 impairment/blockade of the acquired reflex (Fig 8B) and a decrease in VOR gain even  
415 with similar CFs discharges observed during VOR adaptation.

416

417 **Figure 8. Purkinje complex spike-pause frequency and VOR gain error during**  
418 **adaptation and post/pre adaptation. (A) The frequency of Purkinje complex spike-**  
419 **pauses diminishes through VOR adaptation from 8-9 Hz to 1-2 Hz under a sinusoidal**  
420 **vestibular stimulus of ~1 Hz. After VOR adaptation, a direct random stimulation of CFs**  
421 **at 7 Hz during 30 min as in [46] impairs the VOR reflex. (B) Evolution of the VOR gain**

422 *error (Mean Absolute Error) during adaptation, post-adaptation, and artificial random*  
423 *stimulation of CFs.*

424

425 **Discussion**

426 Marr and Albus theory [47, 48] elicited a large body of research on the link between the  
427 cellular and network properties of the cerebellum and behavioural adaptation. This  
428 extensive effort crystallised into a broad range of cerebellar models based on divergent  
429 premises. On the one hand, detailed models were grounded on cellular and synaptic  
430 properties observed experimentally [49-54]. Most of these biophysical models did not  
431 aim at driving behavioural adaptation explicitly through network-level dynamics. On the  
432 other hand, numerous large-scale solutions were engineered to be computationally  
433 efficient for learning sensorimotor tasks, regardless of the anatomo-functional  
434 constraints governing cellular and network cerebellar processes [55-58]. The approach  
435 presented here conjugates these two vantage points and focuses on the role of the  
436 multiple spiking patterns of Purkinje cells in cerebellar adaptation. It is well known that  
437 Purkinje cells can express fast tonic firing as well as a characteristic burst-pause spiking  
438 pattern in response to excitatory parallel fibre (PF) and climbing fibre (CF) inputs [40].  
439 Nevertheless, we address the still uncovered question of how these different spiking  
440 patterns regulate the inhibitory action of Purkinje cells onto targeted medial vestibular  
441 nuclei (MVN) and ultimately shape the adaptive behavioural control mediated by the  
442 cerebellum.

443 We model cerebellar-dependent adaptation of the rotational vestibulo-ocular  
444 reflex (VOR) (Fig 1A). For natural head rotation frequencies (0.5–5.0 Hz), the VOR  
445 gain (i.e., eye velocity divided by head velocity) and the VOR phase shift (i.e., the time

446 lag between eye and velocity profiles) are close to 1 and 180°, respectively [7]. Thus,  
447 synchronised counter-phased eye and head movements stabilise visual targets on the  
448 fovea, minimising retina slips and improving visual acuity [59]. Cerebellar learning, and  
449 particularly Purkinje cell response adaptation, is necessary to mediate online changes in  
450 VOR gain control [60, 61]. The cerebellar model presented here mimics the main  
451 properties of the cerebellar microcircuit, and it embodies spike-based LTP/LTD  
452 plasticity mechanisms at multiple synaptic sites (Fig 1C). At the core of the spiking  
453 cerebellar network, a detailed single-compartment model of Purkinje cell reproduces the  
454 characteristic tonic, complex spike, and post-complex spike pause patterns [62, 63]. In  
455 order to focus on how CF-evoked spike burst-pause dynamics of Purkinje cell responses  
456 can regulate the adaptive output of the cerebellum, we also use a Purkinje neuron model  
457 that cannot express complex spike firing (i.e., it can only operate in tonic mode). The  
458 main finding of this study is that the CF-evoked spike burst-pause dynamics of the  
459 Purkinje cell is a key feature for supporting both early and consolidated VOR learning.  
460 The model predicts that properly timed and sized Purkinje spike burst-pause sequences  
461 are critical to: (1) gating the contingent association between vestibular inputs (about  
462 head rotational velocity) and MVN motor outputs (to determine counter-rotational eye  
463 movements), mediating an otherwise impaired VOR coarse acquisition; (2) allowing the  
464 LTD/LTP balance at MF-MVN synapses to be accurately shaped for optimal VOR  
465 consolidation; (3) reshaping previously learnt synaptic efficacy distributions for VOR  
466 phase-reversal adaptation. Finally, the model predicts that the reversal VOR gain  
467 discontinuities observed after sleeping periods in-between training sessions [3] are due  
468 to LTD/LTP balance modulations (and in particular LTP blockades) occurring during  
469 REM sleep as a consequence of changes in cerebellar activity.

470 This work assumes a gradually modulated CF activity capable of instructing a  
471 ‘teaching’ signal to Purkinje cells [64]. The type of information conveyed by CFs onto  
472 Purkinje cells (and its potential role in sensorimotor adaptation) is under debate. On the  
473 one hand, CFs have been hypothesised to carry a binary feedback-error signal computed  
474 by IO [65]. On the other hand, recent studies have questioned the hypothesis of a binary  
475 CF signal by demonstrating that the duration of Purkinje cell complex spikes (evoked  
476 by CF afferents) can be accurately adjusted based on information that a binary teaching  
477 signal could not support [14, 15, 66-68]. Our model embraces this second hypothesis. It  
478 must also be noted that the overall assumption about IO-mediated feedback-error  
479 learning has been contrasted by a body of research that focused on the periodic nature  
480 of CF activity. These works put the CF signalling in relation to the timing aspects of  
481 motion [69, 70] and, in particular, to the onset of motion [71]. The controversy about the  
482 nature of CF activity has been further roused by the fact that IO functional properties  
483 have so far not been univocally identified [60, 72-74].

484 The model presented here captures the fact that similar CF discharges occur during  
485 both VOR gain increase and decrease adaptation [75, 76]. CFs encode the retinal slips  
486 that drive VOR adaptation [77]. The direction of retinal slips relative to the vestibular  
487 stimulus induces either an increase or a decrease in VOR gain [78]. Interestingly, the  
488 relation between CF activity and the induction of plasticity at Purkinje cell synapses is  
489 described as a gating mechanism that varies under these two VOR adaptation paradigms  
490 [76]. Furthermore, optogenetic CF stimulation in VOR gain-decrease paradigms suggest  
491 that changes in Purkinje cell complex spike responses do not only depend upon CF  
492 activation [76]. Our cerebellar model accounts for these observations by means of the  
493 mechanism that balances LTD/LTP plasticity at PF-Purkinje cell synapses. During VOR  
494 *gain-increase* adaptation, LTD predominantly blocks LTP at modelled PF-Purkinje cell

495 synapses. This results in a synaptic efficacy decrease as a CF spike reaches the target  
496 Purkinje cell (error-related signal). In particular, a CF spike is more likely to depress a  
497 PF-Purkinje cell synapse if the PF has been active within 50-150 ms of the CF spike  
498 arrival [79-81]. Increasing LTD at PF-Purkinje cell synapses reduces the inhibitory  
499 action of Purkinje cells on MVN activity, which in turn increases the VOR gain. During  
500 VOR *gain-decrease* adaptation [25, 75], LTP dominates at PF-Purkinje cell synapses,  
501 despite the fact that CF inputs are similar to those occurring during gain-increase phases.  
502 A raise in synaptic efficacy at PF-Purkinje cell synapses increases the inhibition of MVN  
503 neurons, which in turn reduces the VOR gain. LTP at modelled PF-Purkinje cell  
504 synapses is non-supervised and it strengthens a connection upon each PF spike arrival at  
505 the target Purkinje cell. This plasticity mechanism does not need to modulate the input  
506 provided by CFs (and then the CF-evoked spike burst-pause dynamics of Purkinje cells)  
507 to counter LTD and decrease the VOR gain, in accordance to in-vitro experiments [82-  
508 84].

509 The model suggests that CF-evoked Purkinje cell spike burst-pause dynamics are  
510 critical to shape MF-MVN synapses, as to optimise the accuracy and consolidation rate  
511 of VOR adaptation. We show that burst and spike pause sequences facilitate sparser MF-  
512 MVN connections, which increases coding specificity during the adaptation process.  
513 The results predict that the spike burst-pause dynamics should be central to retune MF-  
514 MVN synapses during VOR phase-reversal adaptation. First, it is shown that blocking  
515 complex spike responses (and post-complex spike pauses) in Purkinje cells impairs  
516 reverse VOR adaptation. More strikingly, the results indicate that Purkinje cell bursting  
517 and spike pauses ensure the reversibility of the adaptation process at MF-MVN synapses.  
518 Bursts selectively facilitate LTD at MF-MVN connections, which rapidly erases  
519 previously learnt memory traces at these synapses. Subsequently, post-complex spike

520 pauses induce strong LTP at MF-MVN synapses, which allows the cerebellar output to  
521 become rapidly reverse-correlated to the sensed error. In addition, the memory  
522 consolidation of VOR adaptation during sleeping [3, 85, 86] is also supported by the CF-  
523 evoked Purkinje cell spike burst-pause dynamics. CF stochastically activations at a low  
524 frequency (0.9 Hz) during REMs stages maintain a base Purkinje bursting that ultimately  
525 facilitates LTP blockades at PF-Purkinje cell and MF-MVN synapses, and it preserves  
526 the on-going learning process.

527 The cerebellar model endowed with CF-evoked Purkinje cell spike burst-pause  
528 dynamics performs better, in terms of adaptation accuracy and consolidation rate, than  
529 a model with Purkinje cells expressing tonic firing only. CF-evoked spike burst-pause  
530 patterns appear particularly useful in a disruptive task such as VOR phase-reversal  
531 adaptation. Nevertheless, our results indicate that complex spikes, post-complex spike  
532 pauses, and their relative modulation, are not essential for VOR control learning and  
533 adaptation. This is in agreement with recent experimental findings challenging the  
534 hypothesis that Purkinje cell complex spikes are necessarily required in cerebellar  
535 adaptation, and suggesting that their role in motor learning is paradigm dependent [74,  
536 87]. Overall, this work provides insights on how the signals provided by the CFs may  
537 instruct, either directly or indirectly, plasticity at different cerebellar synaptic sites [64].  
538 The results point towards a key role of CF-evoked Purkinje cell spike burst-pause  
539 dynamics in driving adaptation at downstream neural stages. This testable prediction  
540 may help to better understanding the cellular-to-network principles underlying  
541 cerebellar-dependent sensorimotor adaptation.

542 **Materials & Methods**

543 **VOR Analysis and Assessment**

544 We simulated horizontal VOR (h-VOR) experiments with mice undertaking sinusoidal  
545 (~1 Hz) whole body rotations in the dark [36]. The periodic functions representing eye  
546 and head velocities (Fig 1A) were analysed through a discrete time Fourier transform.  
547 The **VOR gain** was calculated as the ratio between the first harmonic amplitudes of the  
548 forward Fourier eye– and head–velocity transforms:

549 
$$VOR\ GAIN\ G = \frac{A_I^{eye-velocity}}{A_I^{head-velocity}} \quad (1)$$

550 In order to assess the **VOR shift phase**, the cross-correlation of the eye and head  
551 velocity time series was computed:

552 
$$xcorr = (x * y)[\gamma] \stackrel{def}{=} \sum_{n=-\infty}^{+\infty} x^*(n)y(n+\gamma) \quad (2)$$

553 where  $x^*$  is the complex conjugate of  $x$ , and  $\gamma$  the lag (i.e. shift phase). The ideal eye  
554 and head velocity lag is  $\pm 0.5$  after normalisation, with cross-correlation values ranged  
555 within  $[-1, 1]$ , which is equivalent to a phase shift interval of  $[-360^\circ, 360^\circ]$ .

556 **Cerebellar Spiking Neural Network Model**

557 The cerebellar circuit was modelled as a feed-forward loop capable of compensating  
558 head movements by producing contralateral eye movements (Fig 1B). The connectivity  
559 and the topology of the simulated cerebellar network involved five neural populations:  
560 mossy fibres (MFs), granule cells (GCs), medial vestibular nuclei (MVN), Purkinje  
561 cells, and inferior olive (IO) cells [29, 88-91]. During simulated 1 Hz head rotations,  
562 sensorimotor activity was translated into MF activity patterns that encoded head

563 velocity. MFs transmitted this information to both MVN and GCs. The latter generated  
564 a sparse representation of head velocity signals, which was sent to Purkinje cells through  
565 the PFs. Purkinje cells were also driven by the CFs, which conveyed the teaching signal  
566 encoding sensory error information (i.e., retina slips due to the difference between actual  
567 and target eye movements, [77]). Finally, Purkinje cells' output inhibited MVN neurons,  
568 which closed the loop by shaping cerebellar-dependent VOR control. The CF-Purkinje  
569 cell-MVN subcircuit was divided in two symmetric micro-complexes for left and right  
570 h-VOR, respectively. The input-output function of the cerebellar network model was  
571 made adaptive through spike-timing dependent plasticity (STDP) at stake at multiple  
572 sites (Fig 1C). These STDP mechanisms led to both long-term potentiation (LTP) and  
573 long-term depression (LTD) of the ~50000 synapses of the cerebellar model see [92].  
574 This spiking neural network model was implemented in EDLUT [81, 93, 94] an efficient  
575 open source simulator mainly oriented to real time simulations.

576 ***Purkinje cell model***

577 We considered a detailed Purkinje cell model [62, 63] consisting of a single compartment  
578 with five ionic currents:

$$579 \frac{dV}{dt} = -g_K \cdot n^4 \cdot (V + 95) - g_{Na} \cdot m_0 [V]^3 \cdot h \cdot (V - 50) - \quad (3) \\ -g_{Ca} \cdot c^2 \cdot (V - 125) - g_L \cdot (V + 70) - g_M \cdot M \cdot (V + 95)$$

580 with  $g_K$  denoting a delayed rectifier potassium current,  $g_{Na}$  a transient inactivating  
581 sodium current,  $g_{Ca}$  a high-threshold non-inactivating calcium current,  $g_L$  a leak  
582 current, and  $g_M$  a muscarinic receptor suppressed potassium current (see Table 1).

583

584

585 **Table 1.** Ionic conductance densities

<i>Conductance type</i>	<i>Soma (mho/cm2)</i>
$g_K$ – delayed rectifier potassium current	0.01
$g_{Na}$ – transient inactivating sodium current	0.125
$g_{Ca}$ – high threshold	0.001
$g_M$ – muscarinic receptor	0.75
$g_L$ – leak current (anomalous rectifier)	0.02

586

587 The dynamics of each gating variable evolved as follows:

588

$$\dot{x} = \frac{x_0[V] - x}{\tau_x[V]} \quad (4)$$

589

590 where x indicates the variables n, h, c, and M. The implemented equilibrium function is  
 591 determined by the term  $x_0[V]$  and time constant  $\tau_x[V]$  (Table 2).

592 **Table 2.** Ionic conductance kinetic parameters

<i>Conductance type</i>	<i>Steady-state Activation/Inactivation</i>	<i>Time constant (ms)</i>
$g_K$ – delayed rectifier potassium current	$x_0[V] = \frac{1}{1 + e^{\frac{-V-29.5}{10}}}$	$\tau_x[V] = \begin{cases} 0.25 + 4.35 \cdot e^{\frac{V+10}{10}} & \text{if } V \leq 10 \\ 0.25 + 4.35 \cdot e^{\frac{-V-10}{10}} & \text{if } V > 10 \end{cases}$
$g_{Na}$ – transient inactivating sodium current	$x_0[V] = \frac{1}{1 + e^{\frac{V-59.4}{10.7}}}$	$\tau_x[V] = 0.15 + \frac{1.15}{1 + e^{\frac{V+33.5}{15}}}$
$m_0$ [V]	$m_0[V] = \frac{1}{1 + e^{\frac{-V-48}{10}}} \cdot m$	

	<i>Forward Rate Function</i> ( $\alpha$ )	<i>Backward Rate Function</i> ( $\beta$ )
$g_{Ca}$ -high threshold	$\alpha = \frac{1.6}{1 + e^{-0.0072 \cdot (V - 5)}}$	$\beta = \frac{0.02 \cdot (V + 8.9)}{e^{\frac{V + 8.9}{5}}}$
$g_M$ -muscarinic receptor suppressed potassium current	$\alpha = \frac{0.3}{1 + e^{\frac{-V - 2}{5}}}$	$\beta = 0.001 \cdot e^{\frac{-V - 70}{18}}$
<i>Steady-state Activation/Inactivation</i>		<i>Time constant(ms)</i>
$x_0[V] = \frac{\alpha}{\alpha + \beta}$		$\tau_x[V] = \frac{1}{\alpha + \beta}$

593

594 The sodium activation variable was replaced and approximated by its equilibrium  
 595 function  $m_0[V]$ . M-current presents a temporal evolution significantly slower than the  
 596 rest of the five variables thus provoking a slow-fast system able to reproduce the  
 597 characteristic Purkinje cell spiking modes (Fig 2).

598 The final voltage dynamics for the Purkinje [62, 63]cell model was given by:

$$599 \frac{dV}{dt} = \frac{-g_K \cdot n^4 \cdot (V + 95) - g_{Na} \cdot m_0[V]^3 \cdot h \cdot (V - 50) - g_{Ca} \cdot c^2 \cdot (V - 125) - g_L \cdot (V + 70) - g_M \cdot M \cdot (V + 95) + \frac{\text{Injected Current}}{\text{Membrane Area}}}{\text{Membrane Capacitance}} \quad (5)$$

600

601 where the parameters *Membrane Area* and *Membrane Capacitance* are provided in  
 602 Table 3, and *Injected Current* is the sum of all contributions received through individual  
 603 synapses (see Eqs. 6–8 below).

605

606 **Table 3.** Geometrical parameters:

<i>Geometrical parameters</i>	
Cylinder length of the soma	15 $\mu m$
Radius of the soma	8 $\mu m$
Membrane Capacitance	1 $\mu F/cm^2$
Axial resistivity	100 $\Omega \cdot cm$ (axom) 250 $\Omega \cdot cm$ (dendrites)
Number of segments	1

607

608 First, we validated the detailed Purkinje cell model (Eqs. 3–5) in the Neuron  
609 simulator. Subsequently, we reduced the Purkinje cell model to make it compatible with  
610 an event-driven lookup table (EDLUT) simulator  
611 (<https://github.com/EduardoRosLab/edlut>) for fast spiking neural network simulation  
612 [81, 93]. In the reduced Purkinje cell model,  $I_K$  and  $I_{Na}$  currents were implemented  
613 through a simple threshold process that triggers the generation of a triangular voltage  
614 function each time the neuron fires [95]. This triangular voltage depolarisation drives  
615 the state of ion channels similarly to the original voltage depolarisation during the spike  
616 generation.

617 ***Other cerebellar neuron models***

618 The other cerebellar neurons (granule cells, MVN cells, ...) were simulated as leaky  
619 integrate-and-fire (LIF) neurons, with excitatory (AMPA) and inhibitory (GABA)  
620 chemical synapses:

$$621 C_m \cdot \frac{dV_{m-c}}{dt} = g_{AMPA}(t) \cdot (E_{AMPA} - V_{m-c}) + g_{GABA}(t) \cdot (E_{GABA} - V_{m-c}) + G_{rest} \cdot (E_{rest} - V_{m-c}) \quad (6)$$

622 where  $C_m$  denotes the membrane capacitance,  $E_{AMPA}$  and  $E_{GABA}$  are the reversal potential  
623 of each synaptic conductance,  $E_{rest}$  is the resting potential, and  $G_{rest}$  indicates the  
624 conductance responsible for the passive decay term towards the resting potential.  
625 Conductances  $g_{AMPA}$  and  $g_{GABA}$  integrate all the contributions received by each receptor  
626 type (AMPA and GABA) through individual synapses and they are defined as decaying  
627 exponential functions [81, 96]:

$$628 \quad g_{AMPA}(t) = \begin{cases} 0 & , \quad t \leq t_0 \\ g_{AMPA}(t_0) \cdot e^{-\frac{(t-t_0)}{\tau_{AMPA}}} & , \quad t > t_0 \end{cases} \quad (7)$$

$$629 \quad g_{GABA}(t) = \begin{cases} 0 & , \quad t \leq t_0 \\ g_{GABA}(t_0) \cdot e^{-\frac{(t-t_0)}{\tau_{GABA}}} & , \quad t > t_0 \end{cases} \quad (8)$$

631 with  $t$  representing the simulation time,  $t_0$  being the time arrival of an input spike, and  
632  $\tau_{AMPA}$  and  $\tau_{GABA}$  denoting the decaying time constant for AMPA and GABA receptors,  
633 respectively.

634 Note that we also used the LIF neuronal model (Eqs. 6–8) to simulate Purkinje  
635 cells that could express tonic spike firing only (Fig 3B). These Purkinje cells without  
636 CF-evoked spike burst-pause dynamics provided a coarse phenomenological model  
637 reminiscent of Kv3.3-deficient Purkinje neurons (as in Kcnc3 mutants, in which the  
638 absence of voltage-gated potassium channel Kv3.3 compromises spikelet generation  
639 within complex spikes of cerebellar Purkinje cells) [97]. Table 4 summarises the  
640 parameters used for each cell and synaptic receptor type.

641

642

643

644 **Table 4.** Parameters of the LIF cell types

Parameter	Granule Cell	Purkinje LIF Cell	MVN Cell
Refractory period	1ms	2ms	1ms
Membrane capacitance	2pF	40pF	2pF
*Total excitatory peak conductance	InS·100	1.3nS· ·175000·10%*	InS·7
Total inhibitory peak conductance	InS·200	3nS·150	30nS·1
Threshold	-40mV	-52mV	-40mV
Resting potential	-70mV	-70mV	-70mV
Resting conductance	0.2nS	1.6nS	0.2nS
Resting time constant ( $\tau_{rest}$ )	10ms	25ms	10ms
Excitatory-synapse time constant ( $\tau_{AMPA}$ )	0.5ms	0.5ms	0.5ms
Inhibitory-synapse time constant ( $\tau_{GABA}$ )	10ms	1.6ms	10ms

645

Parameters obtained from the following papers:

646

647 *Granule cell (GC) [98-102]. Only the rapidly decaying component of AMPA is modelled ( $\tau_{AMPA}$   
648  $=0.5ms$ )[103], the presence of slowly decaying components in some GC caused by spillovers of glutamate was  
649 not taken into consideration ( $\tau_{AMPA} =3ms$ )[104]. Purkinje cell (PC) [102, 105-107]. MVN data were extracted  
from unpublished material from Prof. D'Angelo's lab.*

650

\* Where 10% means the ratio of active connections PF-PC (out of the total 175000 PFs)

651

652 **Cerebellar neural population models**

653 Mossy fibres (MFs). N=100 MFs were modelled as LIF neurons (Eqs. 6-8). Consistently  
654 with the functional principles of VOR models of cerebellar control [3], the ensemble  
655 MF activity was generated following a sinusoidal shape (1 Hz with a step size of 0.002  
656 ms) to encode head movements [3, 108, 109]. The overall MF activity was based on non-  
657 overlapping and equally sized neural subpopulations that allowed a constant firing rate  
658 of the ensemble MFs to be maintained over time. Importantly, two different times always

659 corresponded to two different subgroups of active MFs ensuring to the overall constant  
660 activity. (Network connectivity parameters summarised in Table 5).

661 Granular cells (GCs). The granular layer included N=2000 GCs and it was implemented  
662 as a state generator [110-113], i.e. its inner dynamics produced time-evolving states  
663 even in the presence of a constant MF input [56]. The granular layer generated non-  
664 overlapped spatiotemporal patterns that were repeatedly activated in the same sequence  
665 during each learning trial (1 Hz rotation for 1 s)). 500 different states encoded each  
666 second of the 1 Hz learning trial, each state consisting of four non-recursively activated  
667 GCs.

668 Climbing fibres (CFs). N=2 CFs carried the teaching signal (from the IO) to the  
669 population of Purkinje cells. The two CFs handled clockwise and counter-clockwise  
670 sensed errors. CF responses followed a probabilistic Poisson process. Given the  
671 normalised error signal  $\varepsilon(t)$  and a random number  $\eta(t)$  between 0 and 1, a CF fired a  
672 spike if  $\varepsilon(t) > \eta(t)$ , otherwise it remained silent [79, 114, 115]. Thus, a single CF spike  
673 encoded well – timed information regarding the instantaneous error. Furthermore, the  
674 probabilistic spike sampling of the error ensured a proper representation of the whole  
675 error region over trials, while maintaining the CF activity below 10 Hz per fibre (similar  
676 to electrophysiological data; [116]. The evolution of the error could be sampled  
677 accurately even at such a low frequency [115, 117]. For the sake of computational  
678 efficiency, there are only 2 CFs (instead of 20 CFs). In the cerebellum, each PC is  
679 innervated by a single CF [118] coming from the associated IO at the olfactory system.  
680 However, no olfactory system is here considered and, consequently, CFs sensing  
681 clockwise and counter-clockwise errors are equally activated. It would suffice 1 CF  
682 sensing clockwise and 1 CF sensing anti-clockwise errors.

683 Purkinje cells. N=20 Purkinje cells were divided in two subpopulations of 10 neurons  
684 each. Each subpopulation received the inputs from one CF encoding the difference  
685 between (either rightward or leftward) eye and head movements. Each Purkinje cell also  
686 received 2000 PF inputs. Since real Purkinje cells are innervated by about 150000 PFs  
687 [119], the weights of the PF–Purkinje cells synapses of the model were scaled so as to  
688 obtain a biologically plausible amount of excitatory drive. Each of the two subgroups of  
689 10 Purkinje cells targeted (through inhibitory projections) one MVN cell, responsible  
690 for either clockwise or counter-clockwise compensatory motor actions (ultimately  
691 driving the activity of agonist/antagonist ocular muscles).

692 Medial Vestibular Nuclei (MVN). The activity of N=2 MVN cells produced the output  
693 of the cerebellar model. The two MVN neurons handled clockwise and counter-  
694 clockwise motor correction, respectively. Each MVN neuron received excitatory  
695 projections from all MFs (which determined the baseline MVN activity), and inhibitory  
696 afferents from the corresponding group of 10 Purkinje cells (i.e., the subcircuit IO–  
697 Purkinje cell–MVN was organised in a single microcomplex). MVN spike trains were  
698 translated into analogue output signals through a Finite Impulse Response filter (FIR)  
699 [120]. Let  $x(t) = \sum_{j=t}^M \delta(t - t_j)$  denote a MVN spike train, with  $t_j$  being the firing times  
700 of the corresponding neuron. If  $h(t)$  indicates the FIR kernel, then the translated MVN  
701 output is:

$$702 \quad \text{Output}(t) = (h * x)(t) = \sum_{j=t}^M h(t - t_j) \quad (9)$$

703 Note that a delay is introduced in the generated analogue signal. This delay is  
704 related to the number of filter coefficients and to the shape of the filter kernel  $h(t)$ . In  
705 order to mitigate this effect, we used an exponentially decaying kernel:

706

$$Kernel = h(t) = e^{-\frac{M}{\tau_M}} \quad (10)$$

707 where  $M$  is the number of filter taps (one per integration step) and  $\tau_M$  is a decaying factor.

708 At each time step, the output signal value only depends on its previous value and on the  
 709 input spikes in the same time step. Therefore, this filter is implemented by recursively  
 710 updating the last value of the output signal. Importantly, this kernel is similar to  
 711 postsynaptic current functions [121, 122], thus facilitating a biological interpretation.

712 Furthermore, this FIR filter is equivalent to an integrative neuron [123].

713 **Table 5.** Summary of neurons and synapses.

Neurons			Synaptic weights (nS)		
Presynaptic cell number	Postsynaptic cell	Number of synapses	Type	Initial weight (Detailed/non Detailed PC)	Weight range
Mossy Fibres (100)	Granular Cells	8000	AMPA	0.35/0.35*	_____
	Medial Vestibular Nuclei	200	AMPA	0.0/0.0	[0, 10] / [0, 10]
Climbing Fibres (2)	Purkinje Cells	20	AMPA	40/2.5	_____
Granular Cells (1000)	Purkinje Cells	40000	AMPA	3.4/3.75	[0, 3.75] / [0, 5.5]
Purkinje cell (20)	Medial Vestibular Nuclei	20	GABA	0.15/0.15	[0 10] / [0, 10]
Medial Vestibular Nuclei (2)	_____	_____			

714 \* Parameter used for generating the Granular layer activity. Since this activity remained invariant  
 715 during VOR adaptation, it was stored offline in a file and then loaded in computation time.

716

717

718

719 ***Synaptic plasticity rules***

720 *PF–Purkinje cell synaptic plasticity.* The LTD/LTP balance at PF–Purkinje cell  
721 synapses was based on the following rule (S3-1 Fig shows sensitivity analysis  
722 accounting for LTD/LTP balance):

$$723 \quad LTD.\Delta w_{PF_j-PC_i}(t) = \int_{-\infty}^{IO_{spike}} k\left(\frac{t-t_{IO_{spike}}}{\tau_{LTD}}\right) \cdot \delta_{GC_{spike}}(t) \cdot dt \quad \text{if } PF_j \text{ is active at } t \\ 724 \quad LTP.\Delta w_{PF_j-PC_i}(t) = \alpha \cdot \delta_{GC_{spike}}(t) \quad \text{const. otherwise} \quad (11)$$

725 where  $\Delta W_{PF_j-PC_i}(t)$  denotes the weight change between the  $j^{th}$  PF and the target  $i^{th}$   
726 Purkinje cell;  $\tau_{LTD}$  is the time constant that compensates for the sensorimotor delay  
727 (100ms);  $\delta_{GR}$  is the Dirac delta function corresponding to an afferent spike from a PF  
728 (i.e., emitted by a GC); and the kernel function  $k(x)$  is defined as [92]:

$$729 \quad k(x) = e^{-x} \cdot \sin(x)^{20} \quad (12)$$

730 The convolution in Eq. 11 was computed on presynaptic PF spikes arriving 100  
731 ms before a CF spike arrival, accounting for the sensorimotor pathway delay [65, 114,  
732 115, 124]. Note that the kernel  $k(x)$  allows the computation to be run on an event–driven  
733 simulation scheme as EDLUT [81, 114, 115, 124], which avoids integrating the whole  
734 kernel upon each new spike arrival. Finally, as shown in Eq. 11, the amount of LTP at  
735 PF–Purkinje cell synapses was fixed, with an increase in synaptic efficacy equal to  $\alpha$   
736 each time a spike arrived through a PF to the targeted Purkinje cell.

737 *MF–MVN synaptic plasticity.* The LTD/LTP dynamics at MF–MVN synapses was taken  
738 as (Fig. 3-1 shows sensitivity analysis accounting for LTD/LTP balance):

739

$$LTD.\Delta w_{MF_j-MVN_i}(t) = \int_{-\infty}^{+\infty} k\left(\frac{t-t_{PC\_spike}}{\sigma_{MF-MVN}}\right) \cdot \delta_{MF\_spike}(t) \cdot dt \quad \text{if } PC_j \text{ is active at } t \quad (13)$$

$$LTP.\Delta w_{MF_j-MVN_i}(t) = \alpha \cdot \delta_{MF\_spike}(t) \quad \text{const. otherwise}$$

740 with  $\Delta W_{MF_j-MVN_i(t)}$  denoting the weight change between the  $j^{th}$  MF and the target  $i^{th}$  MVN.

741  $\sigma_{MF-DCN}$  standing for the temporal width of the kernel;  $\delta_{MF}$  representing the Dirac delta  
 742 function that defines a MF spike; and the integrative kernel function  $k(x)$  defined as [92]:

743

$$k(x) = e^{-|x|} \cdot \cos(x)^2 \quad (14)$$

744 Note that there is no need to compensate the sensorimotor pathway delay at this  
 745 site because it is already done at PF-Purkinje cell synapses ( $\tau_{LTD}$  in Eq. 11).

746 The STDP rule defined by Eq. 13 produces a synaptic efficacy decrease (LTD)  
 747 when a spike from the Purkinje cell reaches the targeted MVN neuron. The amount of  
 748 synaptic decrement (LTD) depends on the activity arrived through the MFs. This activity  
 749 is convolved with the integrative kernel defined in Eq. (14). This LTD mechanism  
 750 considers those MF spikes that arrive after/before the Purkinje cell spike arrival within  
 751 the time window defined by the kernel. The amount of LTP at MF-MVN synapses is  
 752 fixed (Ito, 1982;[92, 125], with an increase in synaptic efficacy each time a spike arrives  
 753 through a MF to the targeted MVN.

754 Purkinje cell–MVN synaptic plasticity. The STDP mechanism implemented at Purkinje  
 755 cell-MVN synapses [92] consists of a traditional asymmetric Hebbian kernel

756

$$\Delta w_{PC_j-MVN_i}(t) = \begin{cases} LTP \cdot e^{\frac{t_{MVN\_post} - t_{MVN\_pre}}{\sigma_{PC-MVN}^+}} & \text{if } t_{MVN\_post} \geq t_{MVN\_pre} \\ LTD \cdot e^{\frac{t_{MVN\_pre} - t_{MVN\_post}}{\sigma_{PC-MVN}^-}} & \text{otherwise} \end{cases} \quad (15)$$

757 where  $\Delta W_{PCj-MVN_i(t)}$  is the weight change between the  $j^{th}$  PC and the target  $i^{th}$  MVN,  
758  $\sigma_{PC-MVN}^+$  and  $\sigma_{PC-MVN}^-$  are the time constants of the potentiation and depression  
759 components set to 5ms and 15ms respectively ; and  $LTD_{max}/LTP_{max}$  (0.005/0.005 ) are  
760 the maximum weight depression/potentiation change per simulation step. The  $t_{mvn\_post}$   
761 and  $t_{mvn\_pre}$  indicate the postsynaptic and presynaptic MVN spike time. This STDP rule  
762 is consistent with the fact that plasticity at Purkinje cell-MVN synapses depends on the  
763 intensity of MVN and Purkinje cell activities [20-23] and it provides a homeostatic  
764 mechanism in balancing the excitatory and inhibitory cell inputs to MVN [90, 126]. The  
765 source code is available at URL: <http://www.ugr.es/~nluque/restringido/CODE.rar>  
766 (user: REVIEWER, password: REVIEWER).

767

768 *Acknowledgements: This work was supported by the EU NR 658479 SpikeControl, the*  
769 *Spanish Research Project ER CEREBROT TIN2016-81041-R funded by AEI and*  
770 *FEDER, and the ANR – Essilor SilverSight Chair ANR-14-CHIN-0001.*

771 *Financial interests or conflicts of interest statement: The authors declare that the*  
772 *research was conducted in the absence of any commercial or financial relationships that*  
773 *could be construed as a potential conflict of interest*

774 *Author contribution: NRL, ER, and AA conceived the initial idea. FN, RR and NRL*  
775 *designed, modelled and implemented the cerebellar network and the set-up*  
776 *experimentation. NRL and AA prepared figures and drafted the manuscript. All authors*  
777 *reviewed the manuscript and approved the final version.*

778

## 779 References

- 780 1. Ito M. Cerebellar control of the VOR; around the flocculus hypothesis. *Annu Rev*  
781 *Neurosci.* 1982;5(1):275-97.
- 782 2. Herzfeld DJ, Kojima Y, Soetedjo R, Shadmehr R. Encoding of action by the  
783 Purkinje cells of the cerebellum. *Nature.* 2015;526(7573):439-42.
- 784 3. Clopath C, Badura A, De Zeeuw CI, Brunel N. A cerebellar learning model of  
785 VOR adaptation in wild-type and mutant mice. *J Neurosci.* 2014;34(21):7203-15.
- 786 4. Lorente de Nò R. Vestibulo-ocular reflex arc. *Archiv Neurol & Psychiatry.* 1933.
- 787 5. Cohen B. The VOR Arc. In: Kornhuber HH, editor. *Vestibular System Part 1: Basic Mechanisms*: Springer Berlin Heidelberg; 1974. p. 477-540.
- 789 6. Ito M. Error Detection and Representation in the Olivo-Cerebellar System. *Front*  
790 *Neural Circuits.* 2013;1-8.
- 791 7. Leigh RJ, Zee DS. *The neurology of eye movements*: Oxford University Press;  
792 2015.
- 793 8. Medina JF, Lisberger SG. Links from complex spikes to local plasticity and  
794 motor learning in the cerebellum of awake-behaving monkeys. *Nat Neurosci.*  
795 2008;11(10):1185-92.
- 796 9. Welsh JP, Lang EJ, Sugihara I, Llinas R. Dynamic organization of motor control  
797 within the olivocerebellar system. *Nature.* 1995;374(6521):453-7.
- 798 10. Thach WT, Jr. Somatosensory receptive fields of single units in cat cerebellar  
799 cortex. *J Neurophysiol.* 1967;30(4):675-96.
- 800 11. Raman IM, Bean BP. Ionic currents underlying spontaneous action potentials in  
801 isolated cerebellar Purkinje neurons. *J Neurosci.* 1999;19(5):1663-74.
- 802 12. Schmolesky MT, Weber JT, Zeeuw CI, Hansel C. The making of a complex  
803 spike: ionic composition and plasticity. *Ann N Y Acad Sci* 2002;978(1):359-90.
- 804 13. Eccles JC, Llinás R, Sasaki K. The excitatory synaptic action of climbing fibres  
805 on the Purkinje cells of the cerebellum. *J Physiol.* 1966;182(2):268-96.
- 806 14. Najafi F, Medina JF. Beyond "all-or-nothing" climbing fibers: graded  
807 representation of teaching signals in Purkinje cells. *Front Neural Circuits.* 2013;7:1-15.
- 808 15. Mathy A, Ho SS, Davie JT, Duguid IC, Clark BA, Hausser M. Encoding of  
809 oscillations by axonal bursts in inferior olive neurons. *Neuron.* 2009;62(3):388-99.
- 810 16. Najafi F, Giovannucci A, Wang SS-H, Medina JF. Coding of stimulus strength  
811 via analog calcium signals in Purkinje cell dendrites of awake mice. *eLife.* 2014;3. doi:  
812 10.7554/eLife.03663.
- 813 17. Miles F, Lisberger S. Plasticity in the vestibulo-ocular reflex: a new hypothesis.  
814 *Annual review of neuroscience.* 1981;4(1):273-99.
- 815 18. McElvain LE, Bagnall MW, Sakatos A, du Lac S. Bidirectional plasticity gated  
816 by hyperpolarization controls the gain of postsynaptic firing responses at central  
817 vestibular nerve synapses. *Neuron.* 2010;68(4):763-75.

818 19. Menzies JR, Porrill J, Dutia M, Dean P. Synaptic plasticity in medial vestibular  
819 nucleus neurons: comparison with computational requirements of VOR adaptation. *PLoS*  
820 one. 2010;5(10):e13182.

821 20. Aizenman C, Manis P, Linden D. Polarity of long-term synaptic gain change is  
822 related to postsynaptic spike. *Neuron*. 1998;21(4):827-35.

823 21. Morishita W, Sastry B. Postsynaptic mechanisms underlying long-term  
824 depression of gabaergic transmission in neurons of the deep cerebellar nuclei. *J*  
825 *Neurophysiol*. 1996;76(1):59-68.

826 22. Ouardouz M, Sastry B. Mechanisms underlying ltp of inhibitory synaptic  
827 transmission in the deep cerebellar nuclei. *J Neurophysiol* 2000;84(3):1414-21.

828 23. Masuda N, Amari S. A computational study of synaptic mechanisms of partial  
829 memory transfer in cerebellar VOR learning. *J Comput Neurosci*. 2008;24(2):137-56.

830 24. Badura A, Schonewille M, Voges K, Galliano E, Renier N, Gao Z, et al. Climbing  
831 Fiber Input Shapes Reciprocity of Purkinje Cell Firing. *Neuron*. 2013;78(4):700-13.

832 25. Gao Z, vanBeugen BJ, De Zeeuw CI. Distributed Synergistic Plasticity and  
833 Cerebellar Learning. *Nat Rev Neurosci*. 2012;13:1-17.

834 26. Hansel C, Linden DJ, D'Angelo E. Beyond parallel fiber LTD: the diversity of  
835 synaptic and non-synaptic plasticity in the cerebellum. *Nat Neurosci*. 2001;4(5):467-75.

836 27. Garrido JA, Luque NR, D'Angelo E, Ros E. Distributed cerebellar plasticity  
837 implements adaptable gain control in a manipulation task: a closed-loop robotic  
838 simulation. *Front Neural Circuits*. 2013;7.

839 28. Luque NR, Garrido JA, Carrillo RR, D'Angelo E, Ros E. Fast convergence of  
840 learning requires plasticity between inferior olive and deep cerebellar nuclei in a  
841 manipulation task: a closed-loop robotic simulation. *Front Comput Neurosci*. 2014;8.

842 29. Medina JF, Mauk MD. Computer simulation of cerebellar information  
843 processing. *Nat Neurosci*. 2000;3:1205-11.

844 30. D'Angelo E, Mapelli L, Casellato C, Garrido JA, Luque NR, Monaco J, et al. Distributed  
845 Circuit Plasticity: New Clues for the Cerebellar Mechanisms of Learning. *Cerebellum* (London, England). 2015;1-13.

846 31. Shadmehr R, Brashers-Krug T. Functional stages in the formation of human  
847 long-term motor memory. *J Neurosci*. 1997;17(1):409-19.

848 32. Shadmehr R, Holcomb HH. Neural correlates of motor memory consolidation.  
849 *Science*. 1997;277(5327):821-5.

850 33. Ohyama T, Nores WL, Medina JF, Riusech FA, Mauk MD. Learning-induced  
851 plasticity in deep cerebellar nucleus. *J Neurosci*. 2006;26(49):12656-63.

852 34. Kassardjian CD, Tan YF, Chung JY, Heskin R, Peterson MJ, Broussard DM. The  
853 site of a motor memory shifts with consolidation. *J Neurosci*. 2005;25(35):7979-85.

854 35. Anzai M, Kitazawa H, Nagao S. Effects of reversible pharmacological shutdown  
855 of cerebellar flocculus on the memory of long-term horizontal VOR adaptation in  
856 monkeys. *Neurosci Res*. 2010;68(3):191-8.

858 36. Van Alphen AM, Stahl JS, De Zeeuw CI. The dynamic characteristics of the  
859 mouse horizontal vestibulo-ocular and optokinetic response. *Brain Res.*  
860 2001;890(2):296-305.

861 37. McKay BE, Engbers JDT, Mehaffey WH, Gordon GRJ, Molineux ML, Bains JS,  
862 et al. Climbing Fiber Discharge Regulates Cerebellar Functions by Controlling the  
863 Intrinsic Characteristics of Purkinje Cell Output. *J Neurophysiol.* 2007;97(4):2590-604.  
864 doi: 10.1152/jn.00627.2006.

865 38. Llinás R, Sugimori M. Electrophysiological properties of in vitro Purkinje cell  
866 somata in mammalian cerebellar slices. *J Physiol.* 1980;305:171-95.

867 39. Llinás R, Sugimori M. Electrophysiological properties of in vitro Purkinje cell  
868 dendrites in mammalian cerebellar slices. *J Physiol.* 1980;305:197-213.

869 40. Grasselli G, He Q, Wan V, Adelman JP, Ohtsuki G, Hansel C. Activity-  
870 Dependent Plasticity of Spike Pauses in Cerebellar Purkinje Cells. *Cell Reports.*  
871 2016;14(11):2546-53. doi: <http://dx.doi.org/10.1016/j.celrep.2016.02.054>.

872 41. Minor LB, Goldberg JM. Vestibular-nerve inputs to the VOR a functional-  
873 ablation study in the squirrel monkey. *J Neurosci.* 1991;11(6):1636-48.

874 42. Williams JA, Bridgeman B, Woods T, Welch R. Global VOR gain adaptation  
875 during near fixation to foveal targets. *Hum Mov Sci.* 2007;26(6):787-95.

876 43. Gonshor A, Jones GM. Extreme vestibulo-ocular adaptation induced by  
877 prolonged optical reversal of vision. *J Physiol.* 1976;256(2):381-414.

878 44. Mano N. Changes of simple and complex spike activity of cerebellar Purkinje  
879 cells with sleep and waking. *Science.* 1970;170(3964):1325-7.

880 45. Marchesi GF, Strata P. Mossy and climbing fiber activity during phasic and tonic  
881 phenomena of sleep. *Pflügers Archiv.* 1971;323(3):219-40.

882 46. Luebke AE, Robinson DA. Gain changes of the cat's VOR after flocculus  
883 deactivation. *Exp Brain Res.* 1994;98(3):379-90.

884 47. Albus JS. A theory of cerebellar function. *Math Biosci.* 1971;10:25-61.

885 48. Marr D. A theory of cerebellar cortex. *J Physiol.* 1969;202:437-70.

886 49. Solinas S, Nieus T, D'Angelo E. A realistic large-scale model of the cerebellum  
887 granular layer predicts circuit spatio temporal filtering properties. *Front Cell Neurosci.*  
888 2010;4(0).

889 50. Schweighofer N. Computational Models of the Cerebellum in the Adaptive  
890 Control of Movements. PhD thesis. 1995.

891 51. Schweighofer N, Arbib MA, Kawato M. Role of the cerebellum in reaching  
892 movements in human. I. Distributed Inverse dynamics control. *Eur J Neurosci*  
893 1998;10:86-94.

894 52. Schweighofer N, Arbib MA, Kawato M. Role of the cerebellum in reaching  
895 movements in humans.I.Distributed inverse dynamics control. *Eur J Neurosci*  
896 1998a;10:86-94.

897 53. Maex R, De Schutter E. Synchronization of Golgi and granule cell firing in a  
898 detailed network model of the cerebellar granule cell layer. *J Neurophysiol.*  
899 1998;80(5):2521-37.

900 54. Howell FW, Dyhrfjeld-Johnsen J, Maex R, Goddard N, Schutter ED. A large-  
901 scale model of the cereb. cortex using PGENESIS. *Neurocomputing*. 2000;32-3:1041-  
902 6. doi: [http://dx.doi.org/10.1016/S0925-2312\(00\)00277-0](http://dx.doi.org/10.1016/S0925-2312(00)00277-0).

903 55. Tolu S, Vanegas M, Garrido JA, Luque NR, Ros E. Adaptive and Predictive  
904 Control of a Simulated Robot Arm. *Int J Neural Syst.* 2013;23(3).

905 56. Fujita M. Adaptive filter model of the cerebellum. *Biol Cybern.* 1982;45(3):195-  
906 206.

907 57. Porrill J, Dean P. Cerebellar Motor Learning: When Is Cortical Plasticity Not  
908 Enough? *PLOS Comput Biol.* 2007;3(10).

909 58. Tolu S, Vanegas M, Luque NR, Garrido JA, Ros E. Bio-inspired Adaptive FEL  
910 Architecture for Motor Control. *Biol Cybern.* 2012;106(8-9):507-22.

911 59. Blazquez PM, Hirata Y, Heiney SA, Green AM, Highstein SM. Cerebellar  
912 signatures of VOR motor learning. *J Neurosci.* 2003;23(30):9742-51.

913 60. De Zeeuw CI, Simpson JI, Hoogenraad CC, Galjart N, Koekkoek SKE, J. R.  
914 Microcircuitry and function of the inferior olive. *Trends Neurosci.* 1998;21(9):391-400.

915 61. Rambold H, Churchland A, Selig Y, Jasmin L, Lisberger S. Partial ablations of  
916 the flocculus and ventral paraflocculus in monkeys cause linked deficits in smooth  
917 pursuit eye movements and adaptive modification of the VOR. *J Neurophysiol.*  
918 2002;87(2):912-24.

919 62. Middleton SJ, Racca C, Cunningham MO, Traub RD, Monyer H, Knopfel T, et  
920 al. High-frequency network oscillations in cerebellar cortex. *Neuron.* 2008;58(5):763-  
921 74.

922 63. Miyasho T, Takagi H, Suzuki H, Watanabe S, Inoue M, Kudo Y, et al. Low-  
923 threshold potassium channels and a low-threshold calcium channel regulate Ca<sup>2+</sup> spike  
924 firing in the dendrites of cerebellar Purkinje neurons: a modeling study. *Brain Res.*  
925 2001;891(1-2):106-15.

926 64. Ohmae S, Medina JF. Climbing fibers encode a temporal-difference prediction  
927 error during cerebellar learning in mice. *Nat Neurosci.* 2015;18(12):1798-803. doi:  
928 10.1038/nn.4167.

929 65. Kawato M, Gomi H. A computational model of four regions of the cerebellum  
930 based on FEL. *Biol Cybern.* 1992;68(2):95-103.

931 66. Bazzigaluppi P, R. DGJ, Van Der Giessen RS, Khosrovani S, De Zeeuw CI, De  
932 Jeu MTG. Olivary subthreshold oscillations and burst activity revisited *Front Neural  
933 Circuits.* 2012;6(91).

934 67. De Gruijl JR, Bazzigaluppi P, de Jeu MTG, De Zeeuw CI. Climbing Fiber Burst  
935 Size and Olivary Sub-threshold Oscillations in a Network Setting. *PLOS Comput Biol.*  
936 2012;8(12).

937 68. Maruta J, Hensbroek RA, Simpson JI. Intraburst and interburst signaling by  
938 climbing fibers. *J Neurosci.* 2007;27(42):11263-70.

939 69. Llinas R, Welsh JP. On the cerebellum and motor learning. *Curr Opin Neurobiol.*  
940 1993;3:958-65.

941 70. Placantonakis DG, Bukovsky AA, Zeng X-H, Kiem H-P, Welsh JP. Fundamental  
942 role of inferior olive connexin 36 in muscle coherence during tremor. *PNAS*.  
943 2004;101(18):7164-9.

944 71. Keating JG, Thach WT. Nonclock behavior of inferior olive neurons. *Interspike*  
945 interval of Purkinje cell complex spike discharge in the awake behaving monkey is  
946 random. *J Neurophysiol*. 1995;73(4):1329-40.

947 72. Bengtsson F, Hesslow G. Cerebellar control of the inferior olive. *Cerebellum*  
948 (London, England). 2006;review article:1-8.

949 73. Welberg L. Cerebellum: An olive branch to two theories. *Nat Rev Neurosci*.  
950 2009;10:468.

951 74. Popa LS, Streng ML, Hewitt AL, Ebner TJ. The Errors of Our Ways:  
952 Understanding Error Representations in Cerebellar-Dependent Motor Learning.  
953 *Cerebellum* (London, England). 2015.

954 75. Kimpo RR, Boyden ES, Katoh A, Ke MC, Raymond JL. Distinct patterns of  
955 stimulus generalization of increases and decreases in VOR gain. *J Neurophysiol*.  
956 2005;94(5):3092-100.

957 76. Kimpo RR, Rinaldi JM, Kim CK, Payne HL, Raymond JL. Gating of neural error  
958 signals during motor learning. *eLife*. 2014;3:e02076.

959 77. Stone LS, Lisberger SG. Visual responses of Purkinje cells in the cerebellar  
960 flocculus during smooth-pursuit eye movements in monkeys. I. Simple spikes. *J*  
961 *Neurophysiol*. 1990;63(5):1241-61.

962 78. Boyden ES, Katoh A, Raymond JL. Cerebellum-Dependent Learning: The Role  
963 of Multiple Plasticity Mechanisms. *Annu Rev Neurosci*. 2004;27(1):581-609.

964 79. Boucheny C, Carrillo RR, Ros E, Coenen OJ-MD. Real-time spiking neural  
965 network: an adaptive cerebellar model. *LNCS*. 2005;3512:136-44.

966 80. Kettner RE, Mahamud S, Leung H, Sittko N, Houk JC, Peterson BW, et al.  
967 Prediction of complex two-dimensional trajectories by a cerebellar model of smooth  
968 pursuit eye movement. *J Neurophysiol*. 1997;77(4):2115-30.

969 81. Ros E, Carrillo RR, Ortigosa EM, Barbour B, Agís R. Event-driven simulation  
970 scheme for spiking neural networks using lookup tables to characterize neuronal  
971 dynamics. *Neural Comput*. 2006;18(12):2959-93.

972 82. Belmeguenai A, Botta P, Weber JT, Carta M, De Ruiter M, De Zeeuw CI, et al.  
973 Alcohol Impairs LTD at the Cerebellar Parallel Fiber-Purkinje Cell Synapse. *J*  
974 *Neurophysiol*. 2008;100(6):3167-74.

975 83. He Q, Titley H, Grasselli G, Piochon C, Hansel C. Ethanol affects NMDA  
976 receptor signaling at climbing fiber-Purkinje cell synapses in mice and impairs cerebellar  
977 LTD. *J Neurophysiol*. 2013;109(5):1333-42.

978 84. Carey MR, Regehr WG. Noradrenergic Control of Associative Synaptic  
979 Plasticity by Selective Modulation of Instructive Signals. *Neuron*. 2009;62(1):112-22.

980 85. Canto CB, Onuki Yi, Bruinsma B, van der Werf YD, De Zeeuw CI. The Sleeping  
981 Cerebellum. *Trends Neurosci*. 2017.

982 86. Badura A, Clopath C, Schonewille M, De Zeeuw CI. Modeled changes of  
983 cerebellar activity in mutant mice are predictive of their learning impairments. *Sci Rep.*  
984 2016;6:36131.

985 87. Ke MC, Guo CC, Raymond JL. Elimination of climbing fiber instructive signals  
986 during motor learning. *Nat Neurosci.* 2009;12(9):1171-9.

987 88. Eccles JC, Ito M, Szentágothai J. *The Cerebellum as a Neuronal Machine* New  
988 York: Springer-Verlag; 1967.

989 89. Ito M. *The cerebellum and neural control.* 1984.

990 90. Medina J, Mauk M. Simulations of cerebellar motor learning: computational  
991 analysis of plasticity at the mossy fiber synapse. *J Neurosci.* 1999;19(16):7140-51.

992 91. Voogd J, Glickstein M. The anatomy of the cerebellum. *Trends Neurosci.*  
993 1998;21(9):370-5.

994 92. Luque NR, Garrido JA, Náveros F, Carrillo RR, D'Angelo E, Ros E. Distributed  
995 Cerebellar Motor Learning; a STDP Model. *Front Comput Neurosci.* 2016;10. doi:  
996 10.3389/fncom.2016.00017.

997 93. Náveros F, Luque NR, Garrido JA, Carrillo RR, Anguita M, Ros E. A Spiking  
998 Neural Simulator Integrating Event-Driven and Time-Driven Computation Schemes  
999 Using Parallel CPU-GPU Co-Processing: A Case Study. *IEEE Trans Neural Netw Learn  
1000 Syst.* 2015;26(7):1567-74.

1001 94. Náveros F, Garrido JA, Carrillo RR, Ros E, Luque NR. Event-and Time-Driven  
1002 Techniques Using Parallel CPU-GPU Co-processing for Spiking Neural Networks.  
1003 *Frontiers in neuroinformatics.* 2017;11.

1004 95. Bezzi M, Nieuw T, Coenen OJ-M, D'Angelo E. An I&F model of a cerebellar  
1005 granule cell. *Neurocomputing.* 2004;58:593-8.

1006 96. Gerstner W, Kistler WM. *Spiking neuron models: Single neurons, populations,  
1007 plasticity*: Cambridge university press; 2002.

1008 97. Hurlock EC, McMahon A, Joho RH. Purkinje-cell-restricted restoration of Kv3.  
1009 3 function restores complex spikes and rescues motor coordination in KcnC3 mutants. *J  
1010 Neurosci.* 2008;28(18):4640-8.

1011 98. Nusser Z, CullCandy S, Farrant M. Differences in synaptic GABA(A) receptor  
1012 number underlie variation in GABA mini amplitude. *Neuron.* 1997;19:697-709.

1013 99. Rossi DJ, Hamann M. Spillover-mediated transmission at inhibitory synapses  
1014 promoted by high affinity alpha(6) subunit GABA(A) receptors and glomerular  
1015 geometry. *Neuron.* 1998;20:783-95.

1016 100. Silver RA, Colquhoun D, CullCandy SG, Edmonds B. Deactivation and  
1017 desensitization of non-NMDA receptors in patches and the time course of EPSCs in rat  
1018 cerebellar granule cells. *Journal of Physiology.* 1996;493:167-73.

1019 101. Tia S, Wang JF, Kotchabhakdi N, Vicini S. Developmental changes of inhibitory  
1020 synaptic currents in cerebellar granule neurons: Role of GABA(A) receptor alpha 6  
1021 subunit. *Journal of Neuroscience.* 1996;16:3630-40.

1022 102. D'Angelo E, Defilippi G, Rossi P, Taglietti V. Ionic mechanism of  
1023 electroresponsiveness in cerebellar granule cells implicates the action of a persistent  
1024 sodium current. *Journal of neurophysiology.* 1998;80:493-503.

1025 103. Silver RA, Colquhoun D, CullCandy SG, Edmonds B. Deactivation and  
1026 desensitization of non-NMDA receptors in patches and the time course of EPSCs in rat  
1027 cerebellar granule cells. *J Physiol.* 1996;493:167-73.

1028 104. DiGregorio DA, Nusser Z, Silver RA. Spillover of glutamate onto synaptic  
1029 AMPA receptors enhances fast transmission at a cerebellar synapse. *Neuron.*  
1030 2002;35(3):521-33.

1031 105. D'Angelo E, Nieuw T, Maffei A, Armano S, Rossi P. Theta-frequency bursting  
1032 and resonance in cerebellar granule cells: experimental evidence and modeling of a slow  
1033 K<sup>+</sup>-dependent mechanism. *J Neurosci.* 2001;21:759-70.

1034 106. D'Angelo E, Rossi P, Taglietti V. Different proportions of N-Methyl-D-  
1035 Aspartate and Non-N-Methyl-D-Aspartate receptor currents at the mossy fiber granule  
1036 cell synapse of developing rat cerebellum. *Neuroscience.* 1993;53:121-30.

1037 107. Nieuw T, Sola E, Mapelli J, Saftenku E, Rossi P. LTP regulates burst initiation  
1038 and frequency at mossy fiber-granule cell synapses of rat cerebellum: Experimental  
1039 observations and theoretical predictions. *Journal of Neurophysiology.* 2006;95:686-99.

1040 108. Lisberger SG, Fuchs AF. Role of primate flocculus during rapid behavioral  
1041 modification of VOR. II. Mossy fiber firing patterns during horizontal head rotation and  
1042 eye movement. *J Neurophysiol.* 1978;41(3):764-77.

1043 109. Arenz A, Silver RA, Schaefer AT, Margrie TW. The Contribution of Single  
1044 Synapses to Sensory Representation in Vivo. *Science* 2008;321(5891):977-80.

1045 110. Yamazaki T, Tanaka S. The cerebellum as a liquid state machine. *Neural Netw.*  
1046 2007;20:290-7.

1047 111. Yamazaki T, Tanaka S. Computational models of timing mechanisms in the  
1048 cerebellar granular layer. *Cerebellum (London, England).* 2009;8(4):423-32.

1049 112. Yamazaki T, Tanaka S. Neural modeling of an internal clock. *Neural Comput.*  
1050 2005;17(5):1032-58.

1051 113. Honda T, Yamazaki T, Tanaka S, Nagao S, Nishino T. Stimulus-dependent state  
1052 transition between synchronized oscillation and randomly repetitive burst in a model  
1053 cerebellar granular layer. *PLOS Comput Biol.* 2011;7(7):e1002087.

1054 114. Luque NR, Garrido JA, Carrillo RR, Coenen OJMD, Ros E. Cerebellar Input  
1055 Configuration Toward Object Model Abstraction in Manipulation Tasks. *IEEE Trans  
1056 Neural Netw.* 2011;22(8):1321-8.

1057 115. Luque NR, Garrido JA, Carrillo RR, Coenen OJMD, Ros E. Cerebellarlike  
1058 Corrective Model Inference Engine for Manipulation Tasks. *IEEE Trans Syst Man  
1059 Cybern.* 2011;41(5):1299-312.

1060 116. Kuroda S, Yammoto K, Miyamoto H, Doya K, Kawato M. Statistical  
1061 characteristics of climbing fiber spikies necessary for efficient cerebellar learning. *Biol  
1062 Cybern.* 2001;84(3):183-92.

1063 117. Carrillo RR, Ros E, Boucheny C, Coenen O-JM-D. A real time spiking  
1064 cerebellum model for learning robot control. *Biosystems.* 2008;94(1-2):18-27.

1065 118. Kano M, Hashimoto K, Kurihara H, Watanabe M, Inoue Y, Aiba A, et al.  
1066 Persistent Multiple Climbing Fiber Innervation of Cerebellar Purkinje Cells in Mice

1067 Lacking mGluR1. *Neuron*. 1997;18(1):71-9. doi: [https://doi.org/10.1016/S0896-6273\(01\)80047-7](https://doi.org/10.1016/S0896-6273(01)80047-7).

1069 119. Brunel N, Hakim V, Isope P, Nadal JP, Barbour B. Optimal information storage  
1070 and the distribution of synaptic weights: perceptron versus Purkinje cell. *Neuron*.  
1071 2004;43:745-57.

1072 120. Schrauwen B, Van Campenhout J, editors. BSA, a fast and accurate spike train  
1073 encoding scheme. *Neural Netw*, 2003 Proc Int Jt Conf; 2003: IEEE.

1074 121. Victor JD. Spike train metrics. *Curr Opin Neurobiol*. 2005;15(5):585-92.

1075 122. van Rossum MC. A novel spike distance. *Neural Comput*. 2001;13(4):751-63.

1076 123. Luque NR, Carrillo RR, Náveros F, Garrido JA, Sáez-Lara MJ. Integrated neural  
1077 and robotic simulations. Simulation of cerebellar neurobiological substrate for an object-  
1078 oriented dynamic model abstraction process. *Rob Auton Syst*. 2014;62(12):1702-16.

1079 124. Luque NR, Garrido JA, Carrillo RR, Tolu S, Ros E. Adaptive cerebellar spiking  
1080 model embedded in the control loop: Context switching and robustness against noise.  
1081 *Int J Neural Syst*. 2011;21(05):385-401.

1082 125. Lev-Ram V, Mehta SB, Kleinfeld D, Tsien RY. Reversing cerebellar long-term  
1083 depression. *Proceedings of the National Academy of Sciences*. 2003;100(26):15989-93.

1084 126. Kleberg FI, Fukai T, Gilson M. Excitatory and inhibitory STDP jointly tune  
1085 feedforward neural circuits to selectively propagate correlated spiking activity. *Front*  
1086 *Comput Neurosci*. 2014;8.

1087 127. Song S, Miller KD, Abbott LF. Competitive Hebbian learning through spike-  
1088 timing-dependent synaptic plasticity. *Nature neuroscience*. 2000;3(9):919-26.

1089 128. Rubin J, Lee DD, Sompolinsky H. Equilibrium properties of temporally  
1090 asymmetric Hebbian plasticity. *Physical review letters*. 2001;86(2):364.

1091

1092

1093 **Supporting Information**

1094 **Figure Captions**

1095 **Figure S3-1. Critical LTD/LTP balance at PF-Purkinje cell and MF-MVN**

1096 **synapses: sensitivity analysis.** Cerebellar adaptation modulates PF-Purkinje cell  
1097 synaptic weights as well as MF-MVN synapses [6, 92]. For synaptic adaptation, the  
1098 model uses supervised STDP, which exploits the interaction amongst unsupervised and  
1099 supervised cell inputs to regulate and stabilise postsynaptic activity. Balancing  
1100 supervised STDP, and the resulting synaptic modification dynamics, is critical, given  
1101 the high sensitivity of the process that determines the LTD/LTP ratio [127, 128]. A  
1102 sensitivity analysis of the parameters governing LTD and LTP, shows that LTP  
1103 exceeding LTD values for a narrow range at MF-MVN synapses preserves VOR  
1104 learning stability. This holds independently for both VOR gain and phase **(A)** as well as  
1105 for the combination of the two **(B)**. By contrast, PF-Purkinje cell synapses admit broader  
1106 limits for the LTD/LTP ratio **(A, B)**.

1107 *More detailed description:* we systematically simulated LTP/LTD ratio values at PF-  
1108 Purkinje cell and MF-MVN synapses within a plausible range that may satisfy the  
1109 expected h-VOR outcome. As simulations ran, the solutions were iteratively checked  
1110 until finding the set of LTD/LTP ratio values that exhibited the better performance in  
1111 terms of h-VOR gain and phase. LTD/LTP balance at each site was modified by  
1112 systematically multiplying LTD by  $1.5^N$  where  $-11 \leq N \leq 12$  for PF-Purkinje cell and  
1113 MF-MVN synapses. For each parameter setting, the cerebellar model underwent 10 000  
1114 sec of VOR learning (1Hz head rotation movement to be compensated by contralateral  
1115 eye movements. **(A)** Final VOR gain and phase plotted over the LTD/LTP range of  
1116 values that were tested. **(B)** Combined VOR gain and phase (normalised) as a function  
1117 of the LTD/LTP ratio. At PF-Purkinje cell synapses the LTD/LTP was well balanced for

1118 N values ranging between  $[-1, 7]$ . At MF-MVN the LTD/LTP balance was more critical  
1119 since N is within a narrower band range  $[-1, 0]$ . The reddish area within the last plot  
1120 indicates the optimal parameters range. LTP must exceed LTD at MF-MVN synapses  
1121 for optimal VOR performance. This result is consistent with the unsupervised nature of  
1122 the LTP for the kernel defined for MF-MVN STDP. Unsupervised LTP with larger  
1123 values than LTD takes the MF-MVN synaptic weights to the upper bound of their  
1124 synaptic efficacy, thus provoking more MVN activations. In the absence of LTD  
1125 counteraction, the cerebellar output is, therefore, upper saturated. LTD driven by  
1126 Purkinje cell activity blocks LTP at MF-MVN synapses, thus shaping the cerebellar  
1127 compensatory output.

1128 **Figure S3-2. LTD/LTP balance at MF-MVN synapses over time.** Whilst LTD/LTP  
1129 balance was fixed at PF-PC synapses, we modified the LTD/LTP balance at MF-MVN  
1130 synapses by systematically varying the ratio by  $1.5^N$  where  $-11 \leq N \leq 12$  during a 10000  
1131 sec simulation. **(A)** Final VOR gain and phase plotted as a function of the tested  
1132 LTD/LTP range across time. **(B)** Combined VOR gain and phase (normalised) over time.  
1133 A proper balance between LTD and LTP (ratio of approximately 0.4) makes the  
1134 cerebellum perform optimally after 750 sec.

1135 **Figure S3-3. Parameter sensitivity analysis for the LTD/LTP balance at PF-**  
1136 **Purkinje cell and MF-MVN synapses in the absence of Purkinje spike burst-pause**  
1137 **dynamics.** Similar to Fig. 3-1, the parameters regulating the LTD/LTP ratio were  
1138 exhaustively tested whilst the cerebellar model without Purkinje complex spiking  
1139 underwent h-VOR learning during a 10000 sec simulation. **(A)** Final VOR gain and  
1140 phase plotted over the LTD/LTP range of tested values. **(B)** Combined VOR gain and  
1141 phase (normalised) as a function of the LTD/LTP ratio. LTD/LTP at both PF-Purkinje

1142 cell synapses is well balanced for N values ranged between [-1, 7]. Thus, the absence of  
1143 bursting and pause dynamics leads to a wider range values for the LTD/LTP balance.

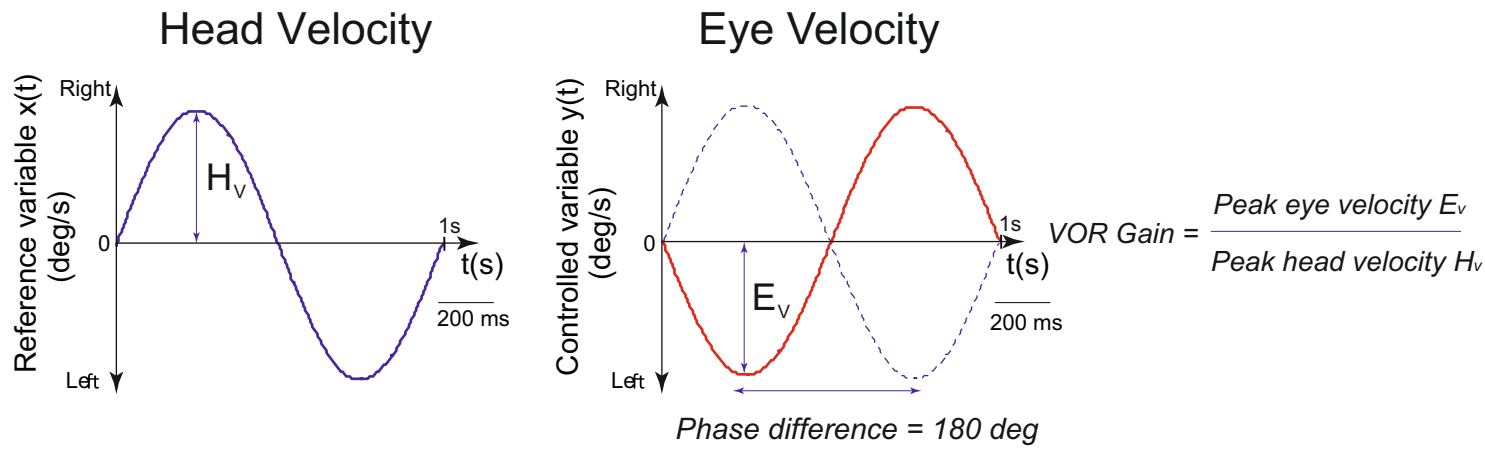
1144 **Figure S5-1. VOR phase-reversal learning: time course of the VOR phase. (A)** VOR  
1145 phase adaptation with (red curve) and without (green curve) Purkinje spike burst-pause  
1146 dynamics. **(B)** Focus is on the phase-reversal period and comparison with experimental  
1147 data [3].

1148 **Figure S6-1. Eye velocity evolution during VOR phase-reversal learning** **(A)** Only  
1149 the eye velocity movement corresponding to the sparser and more selective distribution  
1150 of MF-MVN synaptic weights is able to counteract the head velocity movement in  
1151 counter phase **(B)**, as phase-reversal learning is achieved **(C)**.

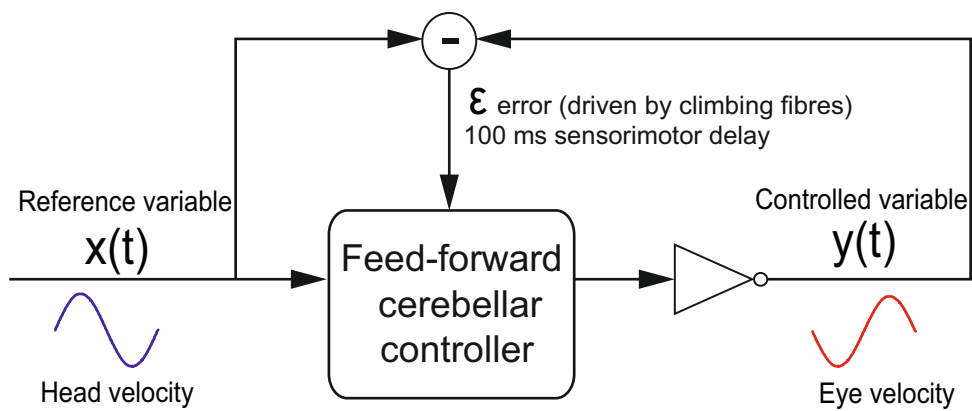
1152 **Figure S7-1. Climbing fibre activation.** In the model, CF responses follow a  
1153 probabilistic Poisson process. Given the normalised error signal  $\varepsilon(t)$  obtained from the  
1154 retina slip and a random number  $\eta(t)$  between 0 and 1, the model CF fires a spike if  
1155  $\varepsilon(t) > \eta(t)$ ; otherwise, it remains silent[79] A single spike is then able to report timed  
1156 information regarding the instantaneous error. Furthermore, the probabilistic spike  
1157 sampling of the error ensures that the entire error region is accurately represented over  
1158 trials with a constrained CF activity below 10 spikes per second, per fibre (CF activated  
1159 between 1-10 Hz). Hence, the error evolution is accurately sampled even at a low  
1160 frequency [115, 117]. This firing behaviour is consistent to those observed in  
1161 neurophysiological recordings [116].

1162

A



B



C

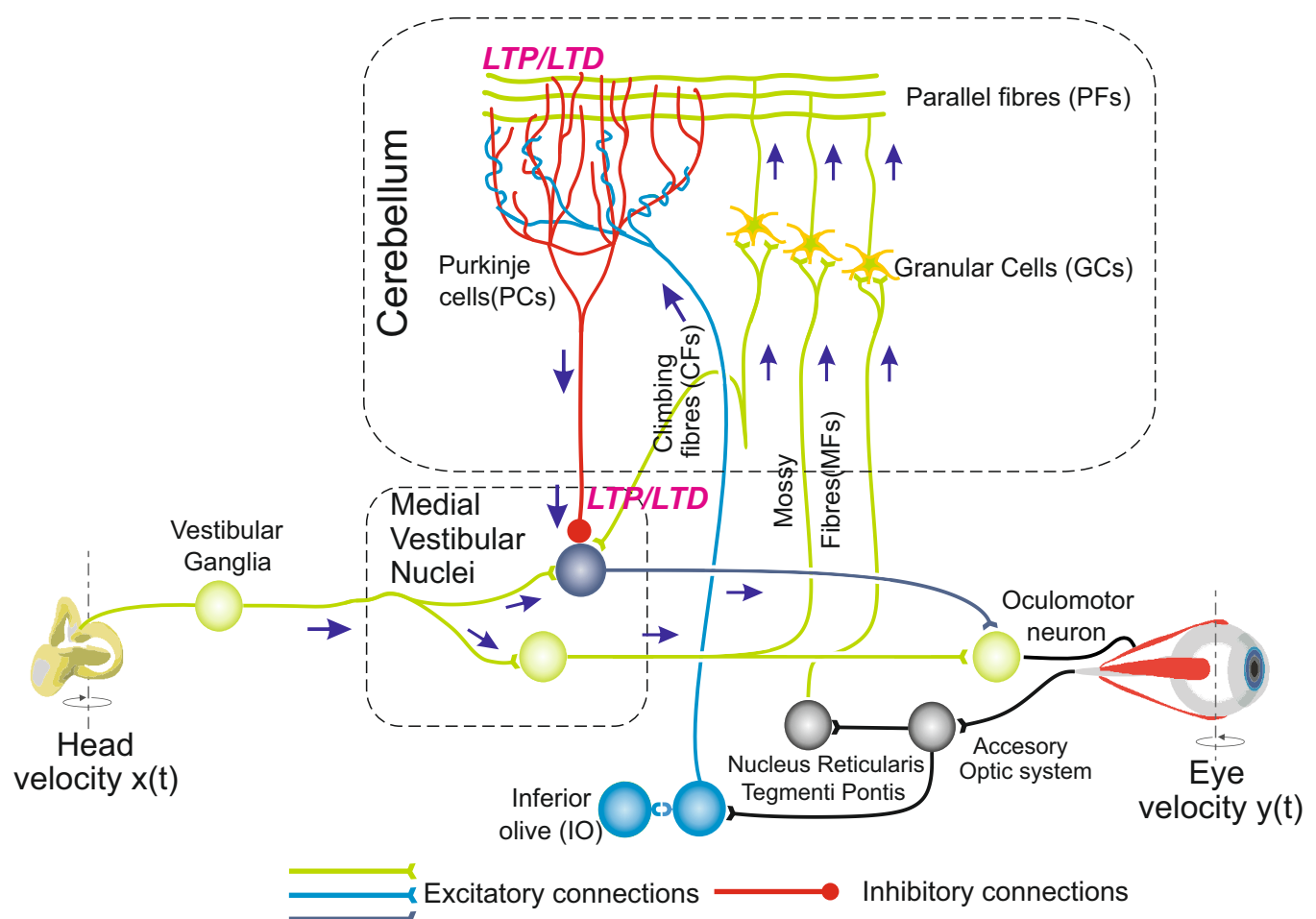
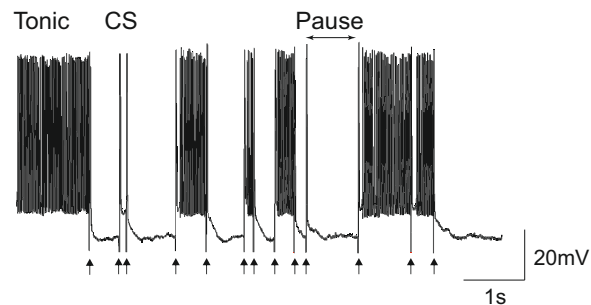
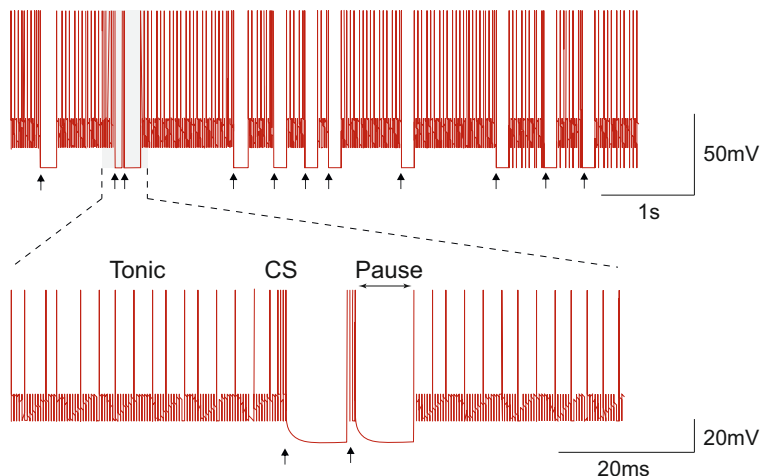
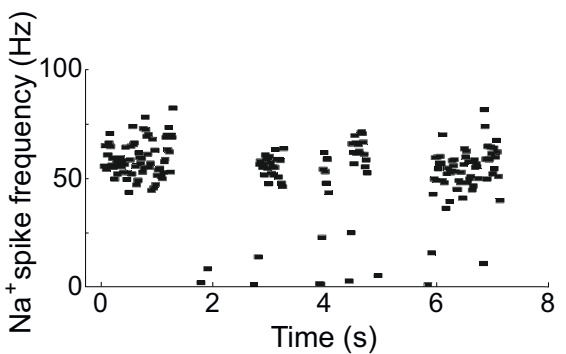
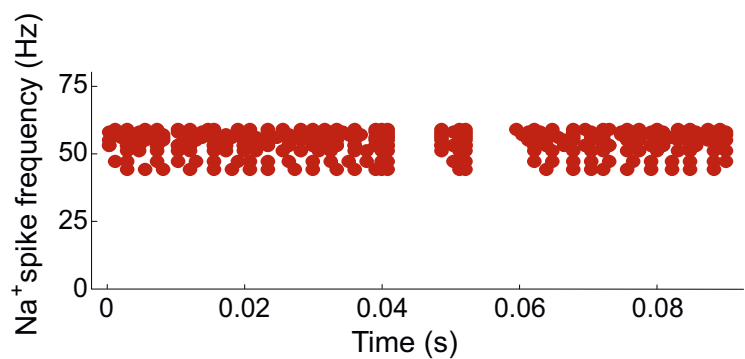


Figure 1

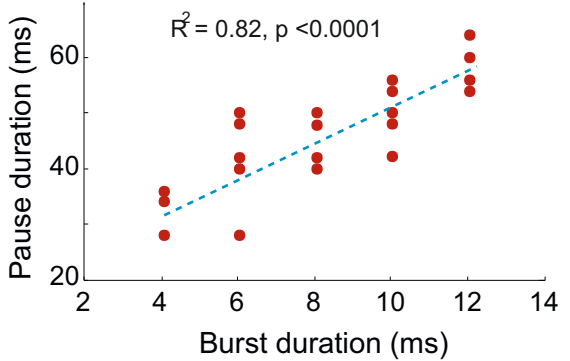
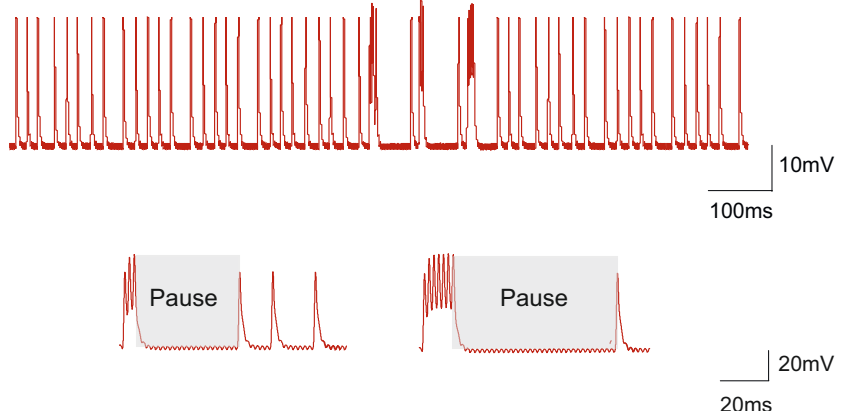
A



B



C



D

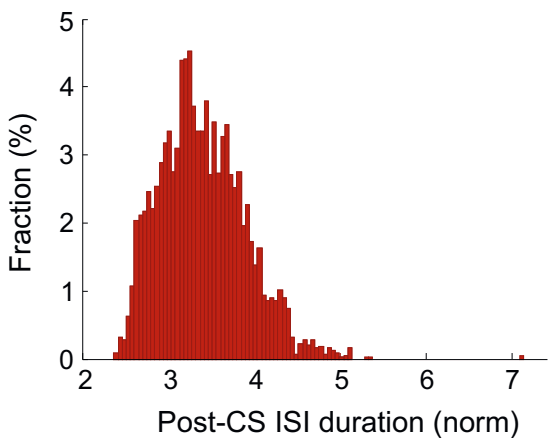
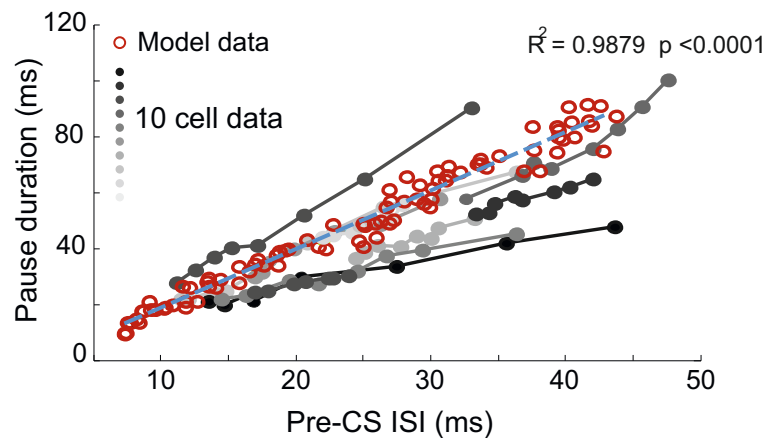
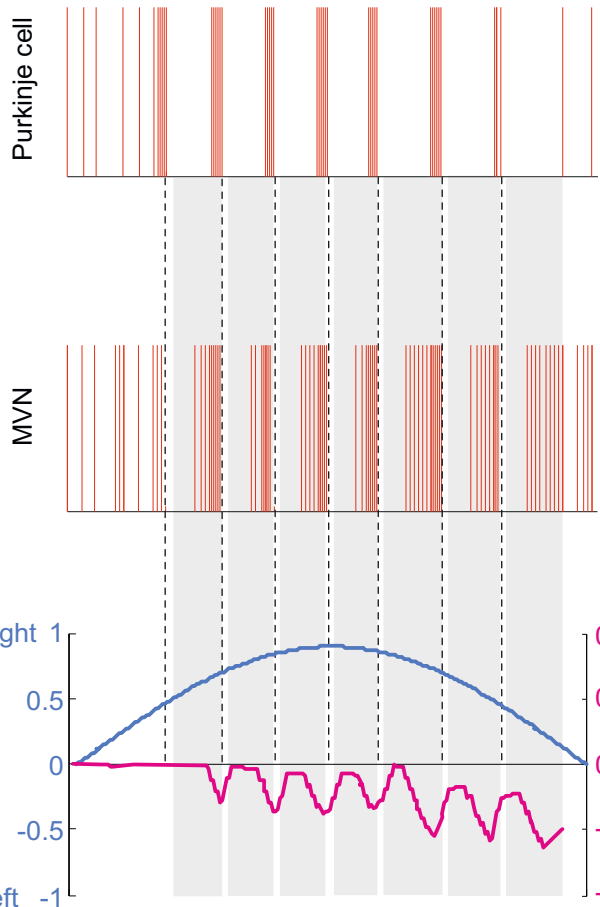


Figure 2

A

CS Purkinje Cell



B

no-CS Purkinje Cell

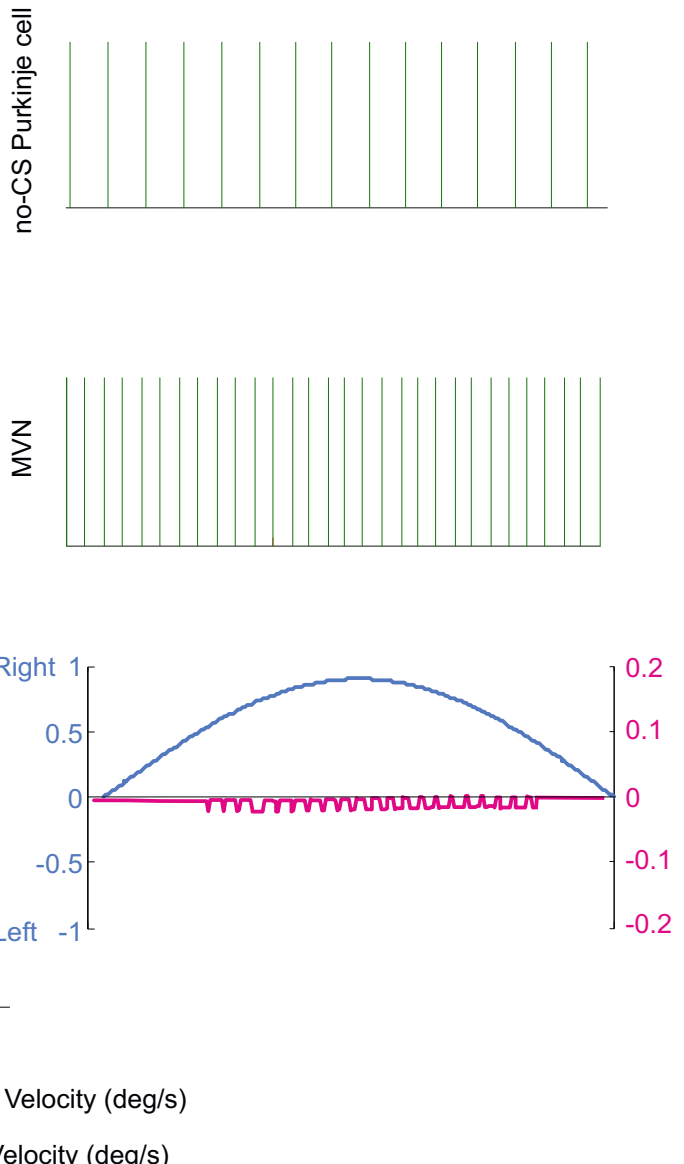
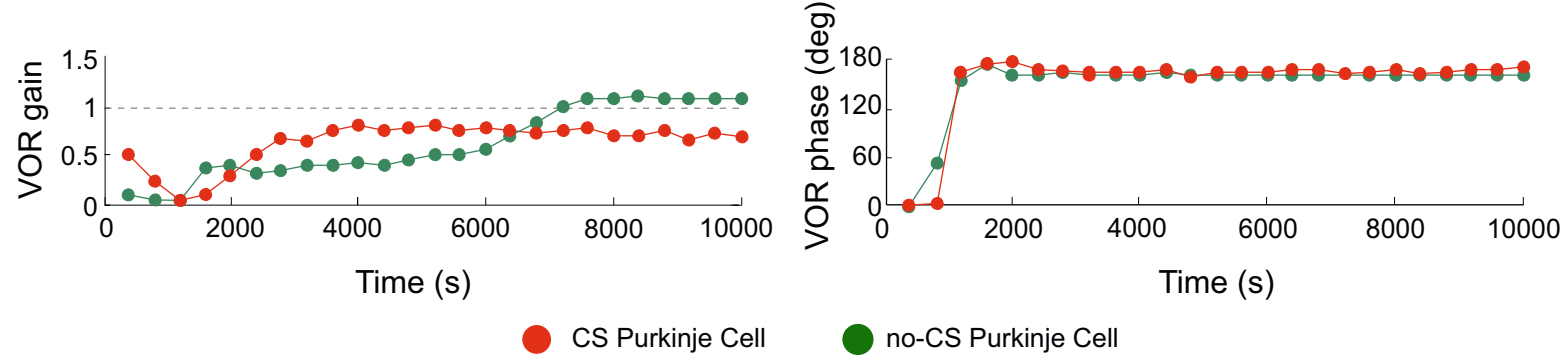


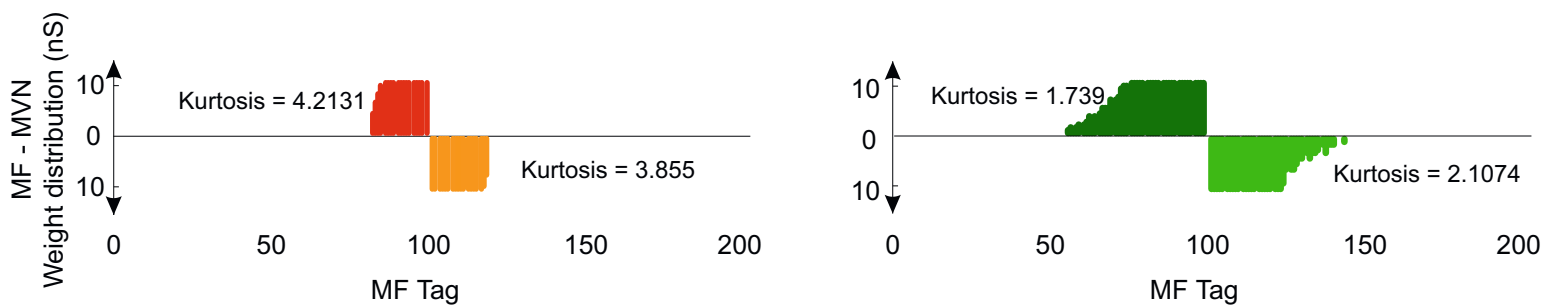
Figure 3

A

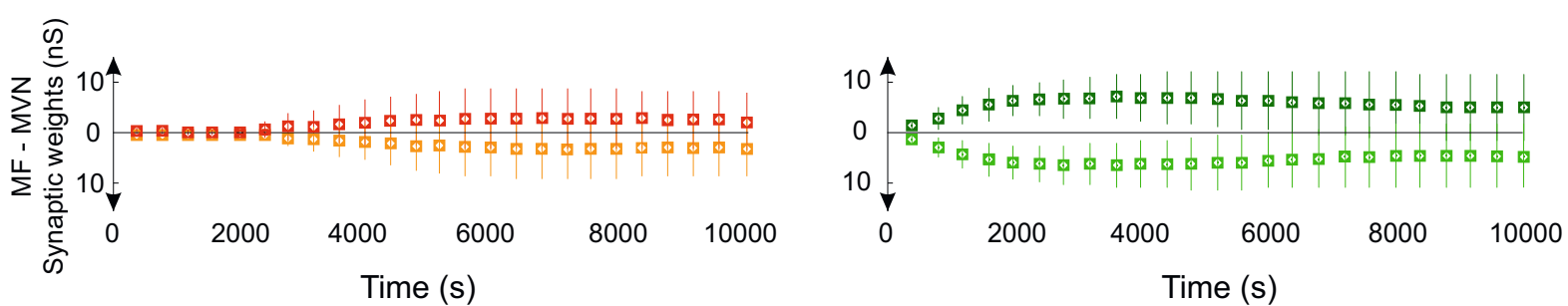


B

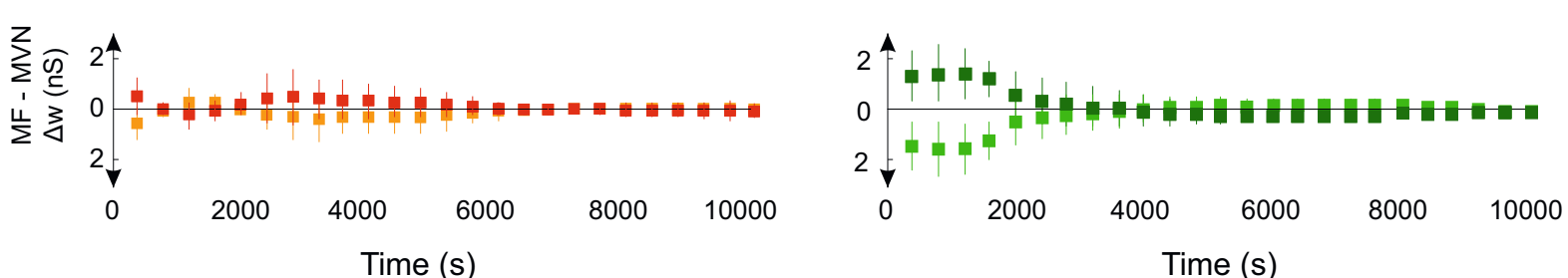
CS Purkinje Cell      no-CS Purkinje Cell



C



D

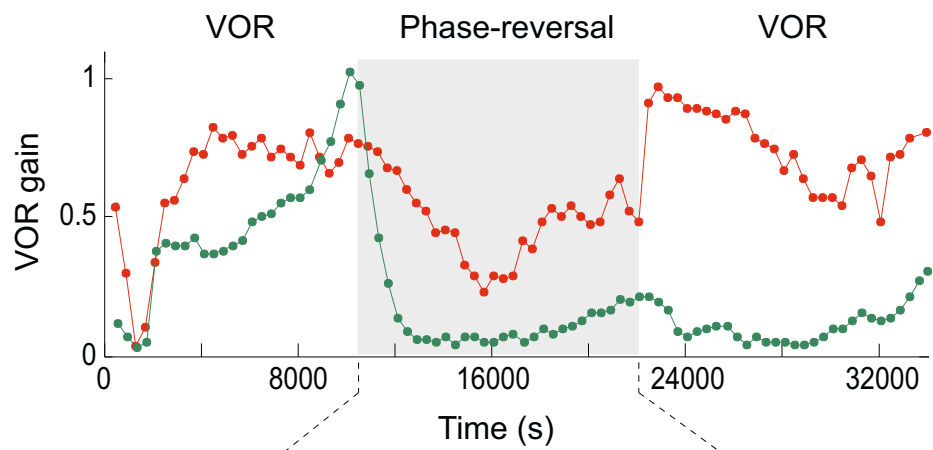


Rightward correction      ■

Leftward correction      ■      ●

Figure 4

A



B

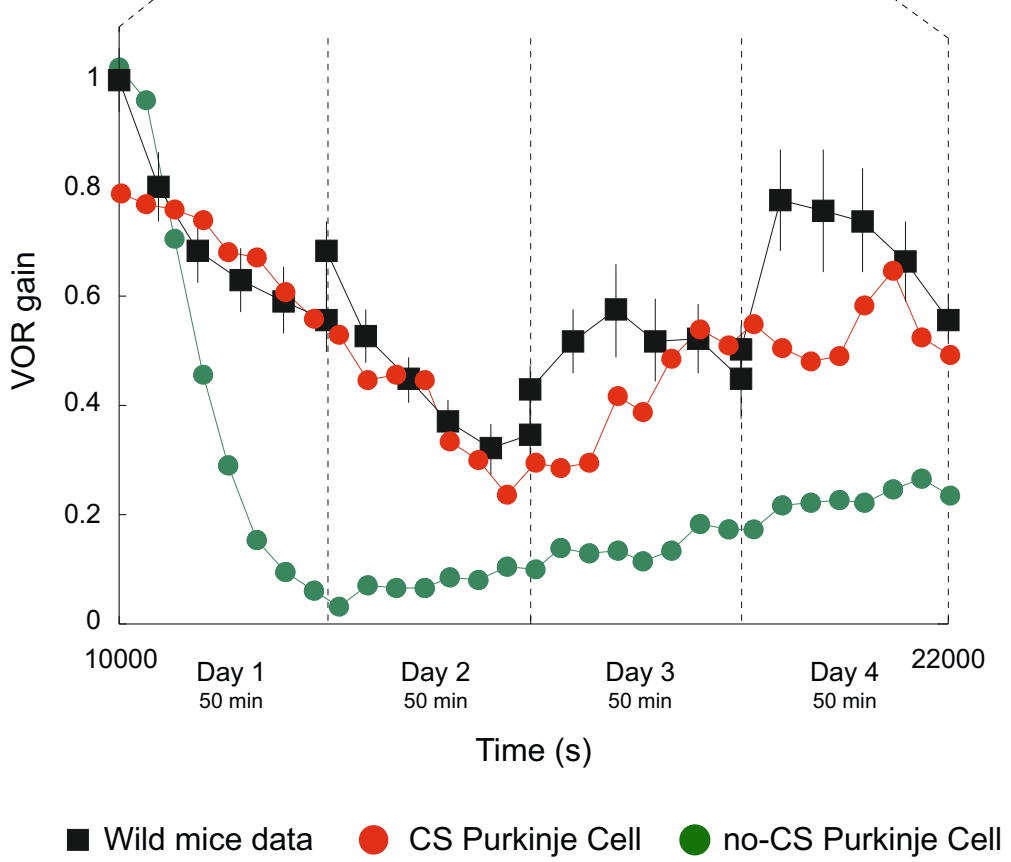
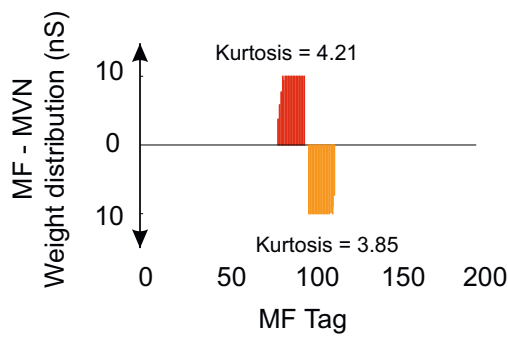


Figure 5

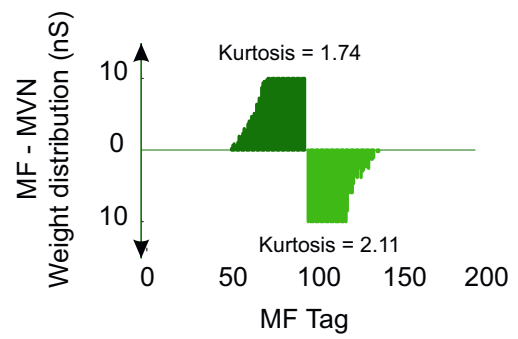
### CS Purkinje Cell

### no-CS Purkinje Cell

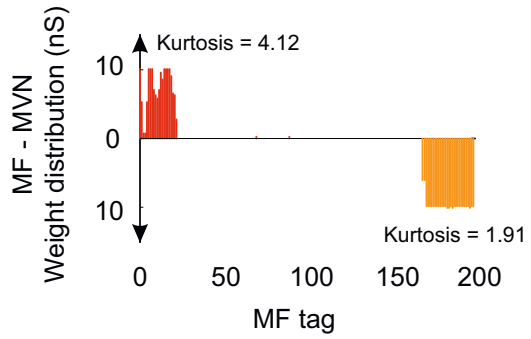
A



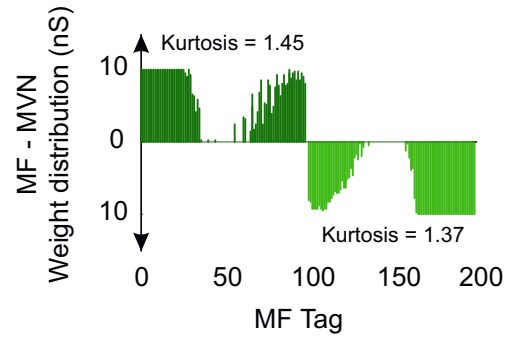
$t=10000$  s



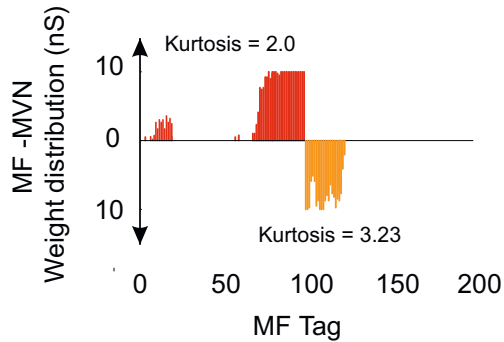
B



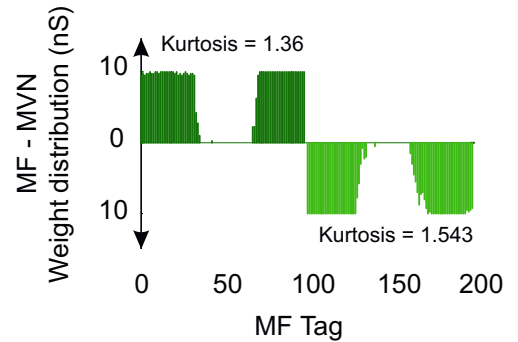
$t=22000$  s



C



$t=32000$  s



Rightward correction ■ ■

Leftward correction □ □

Figure 6

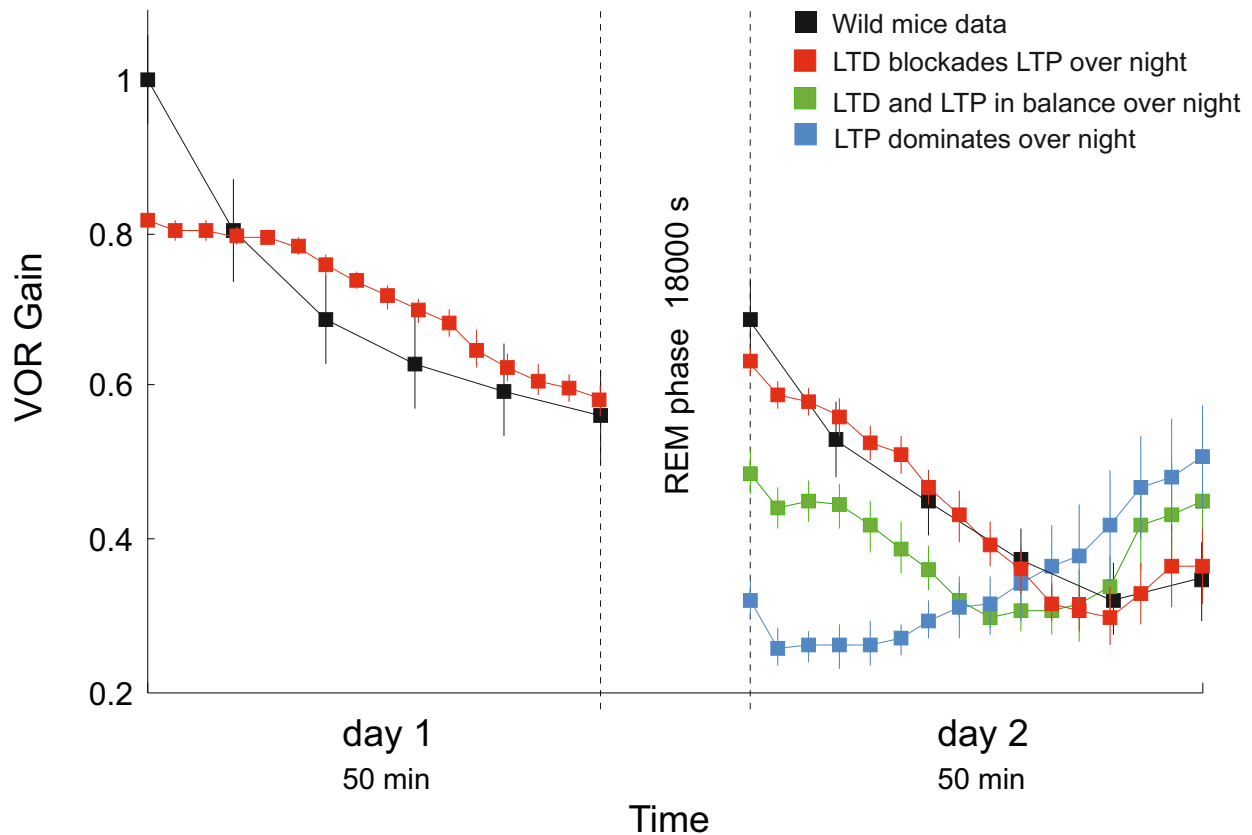
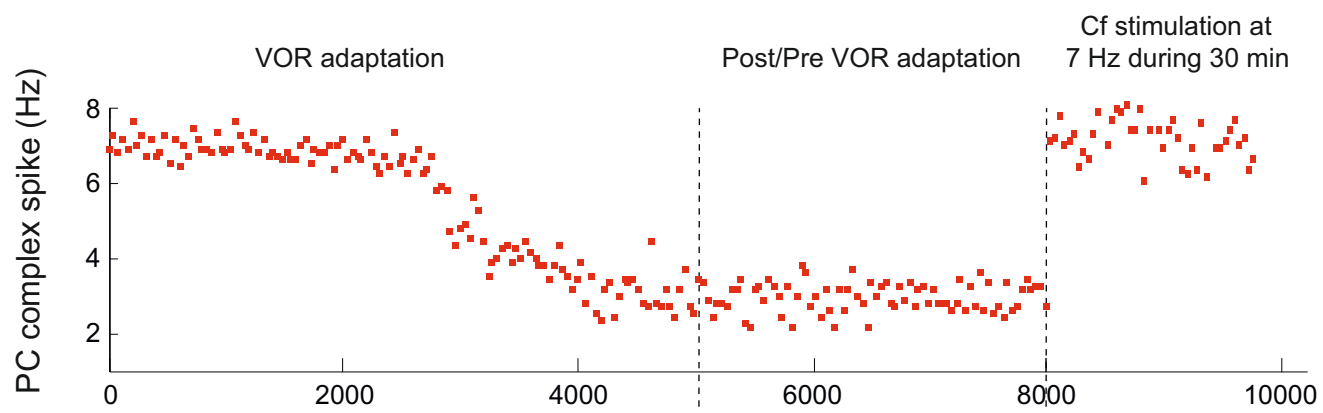


Figure 7

A



B

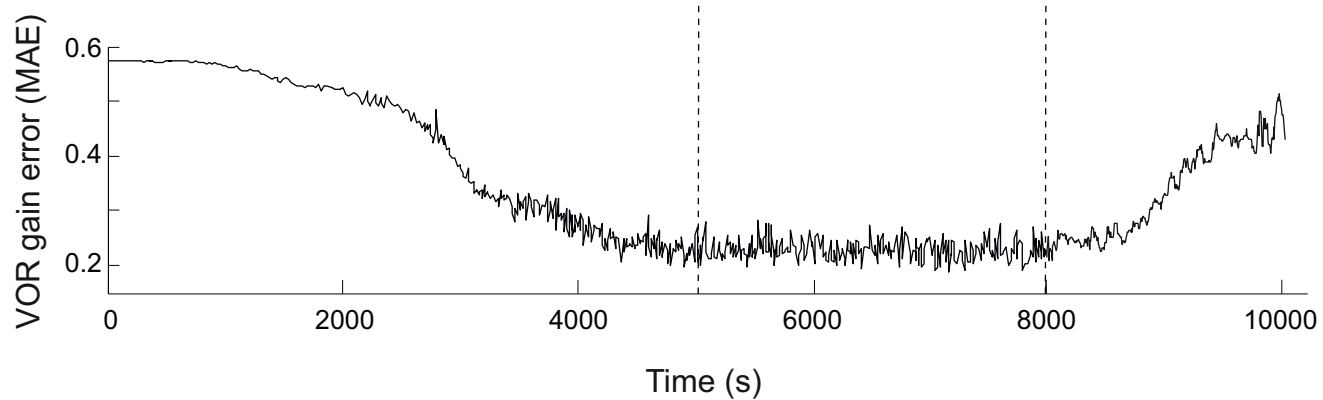
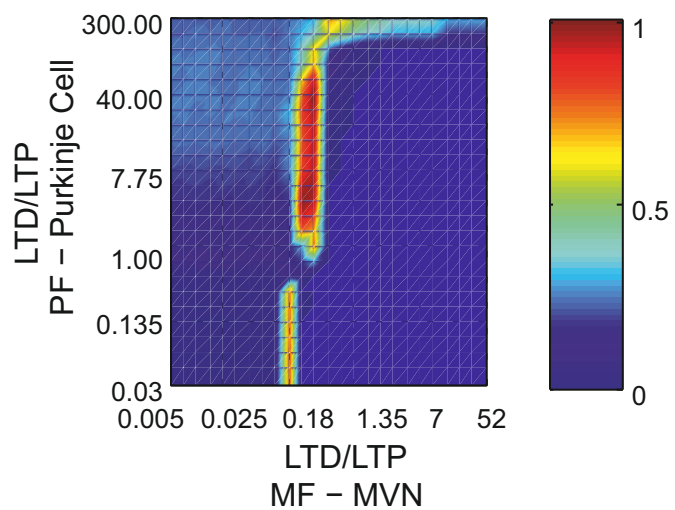


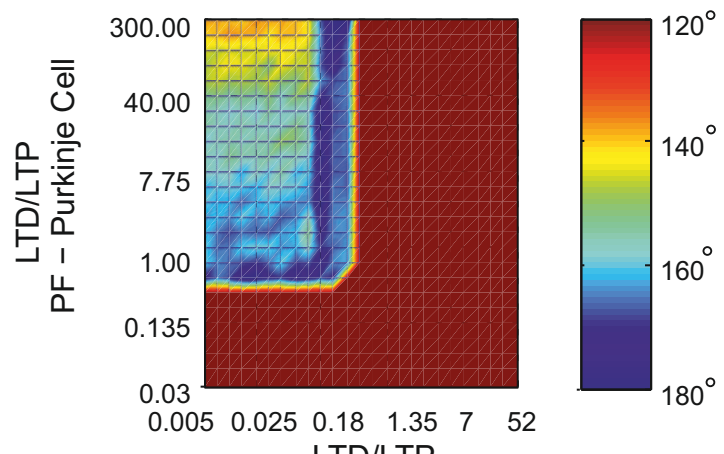
Figure 8

A

VOR Gain



VOR Phase



B

VOR Gain & Phase

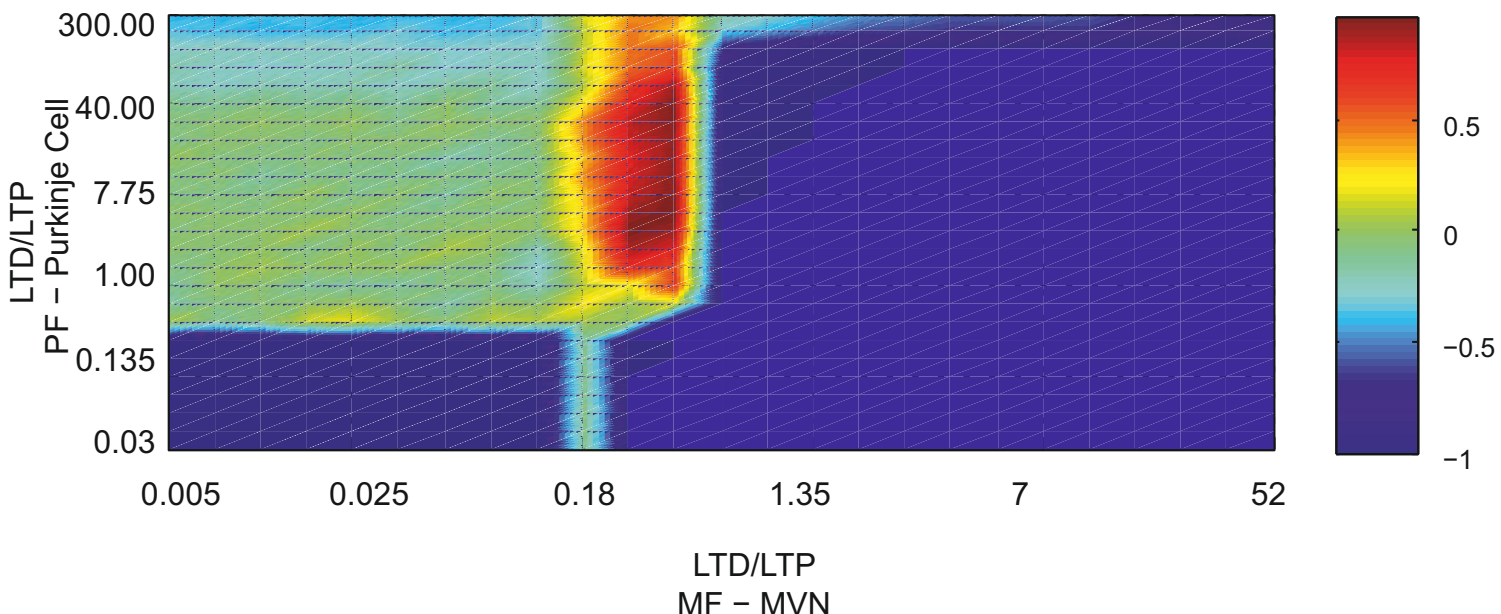
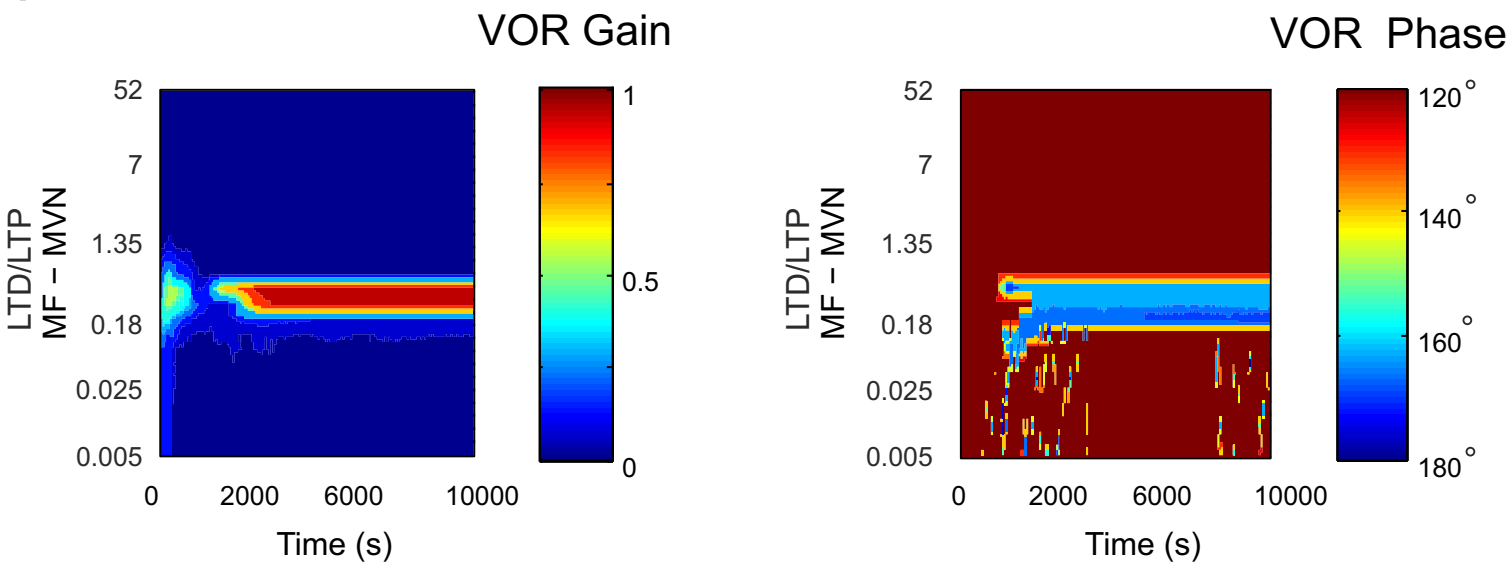


Figure S3-1

A



B

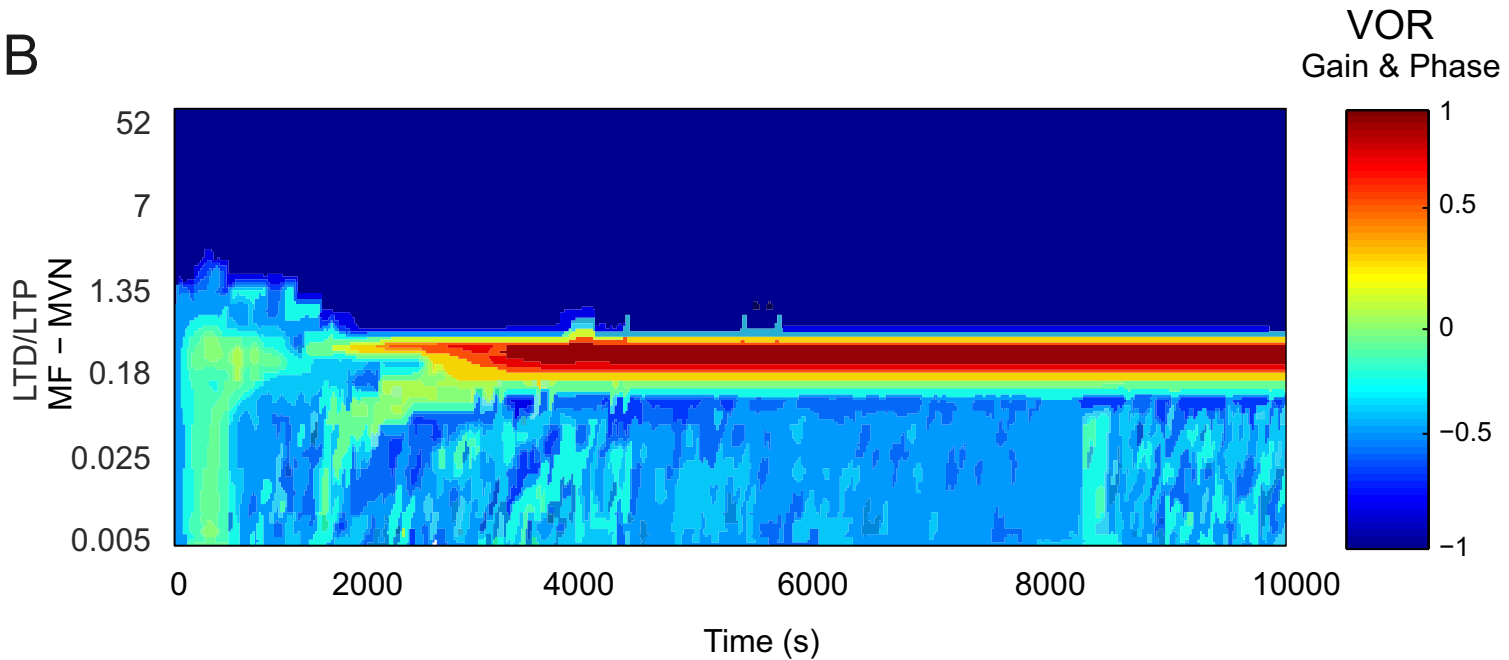
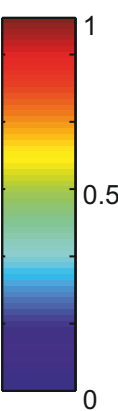
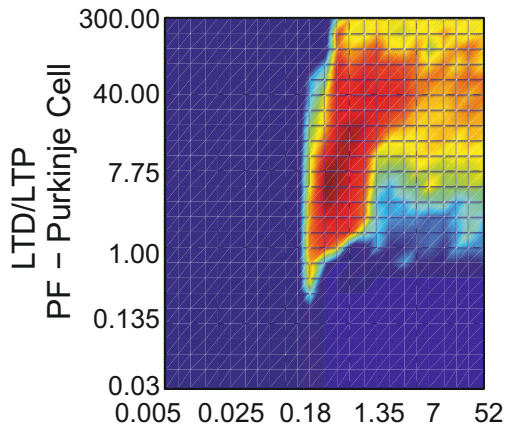


Figure S3-2

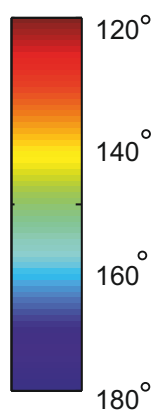
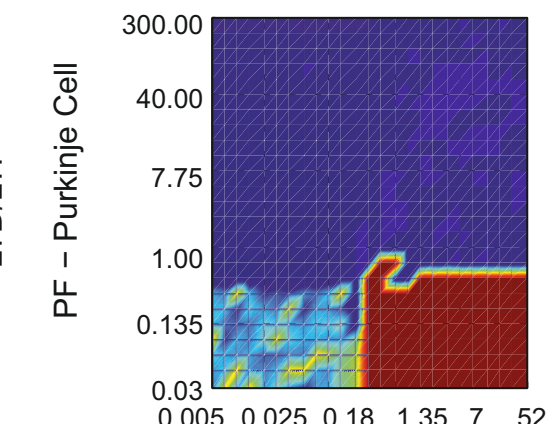
A

bioRxiv preprint doi: <https://doi.org/10.1101/347252>; this version posted June 14, 2018. The copyright holder for this preprint (which was not certified by peer review) is the author/funder, who has granted bioRxiv a license to display the preprint in perpetuity. It is made available under aCC-BY 4.0 International license.

### VOR Gain



### VOR Phase



LTD/LTP  
MF - MVN

LTD/LTP  
MF - MVN

B

### VOR Gain & Phase

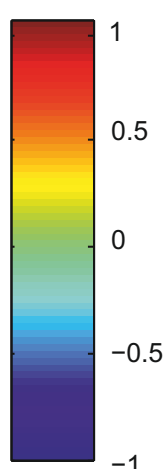
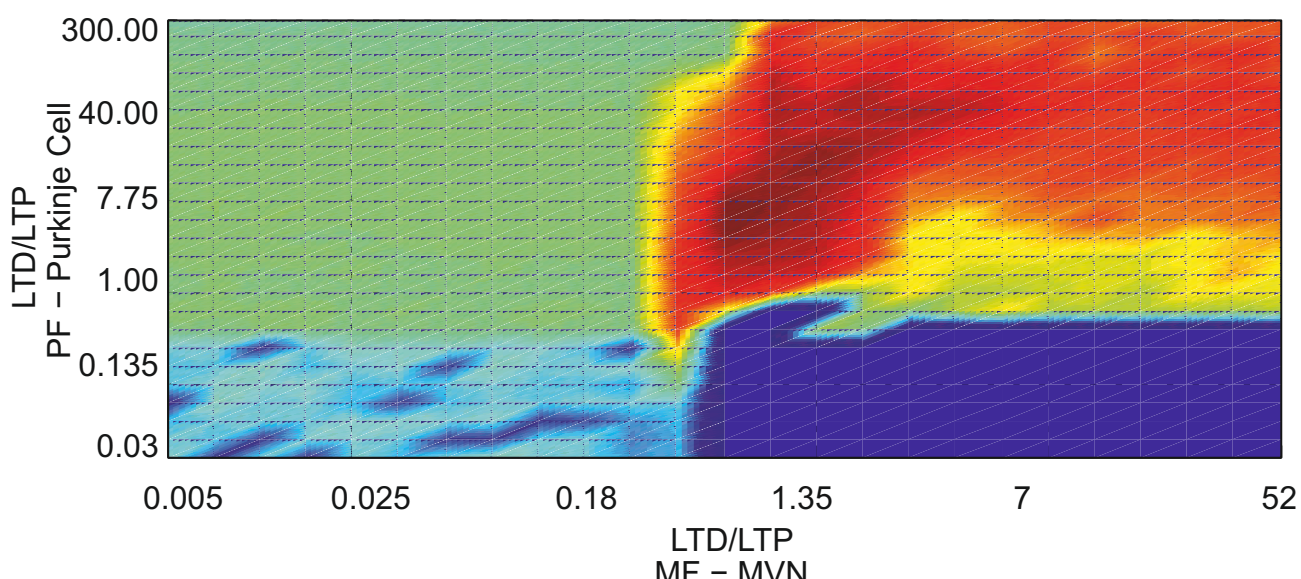


Figure S3-3

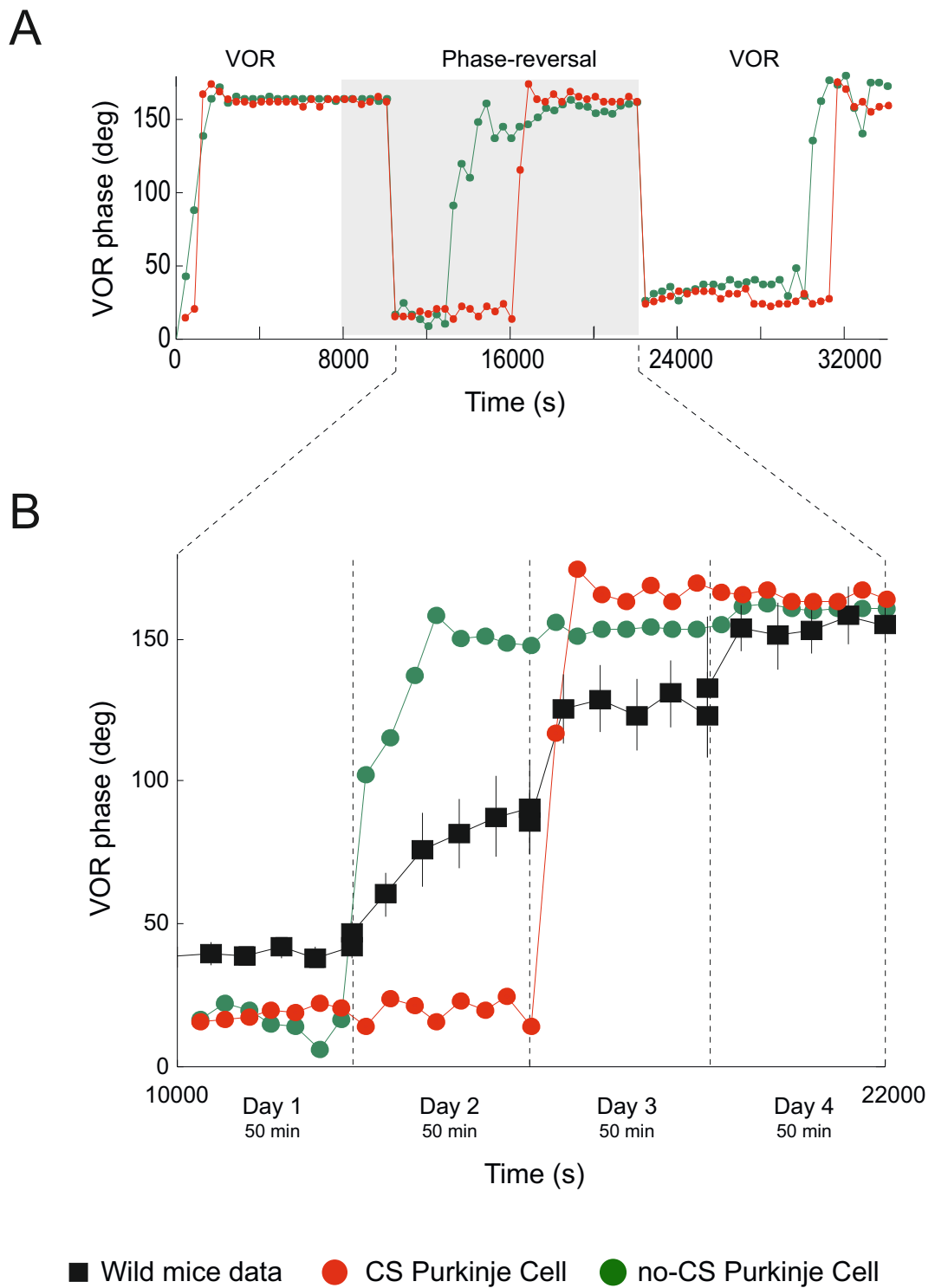
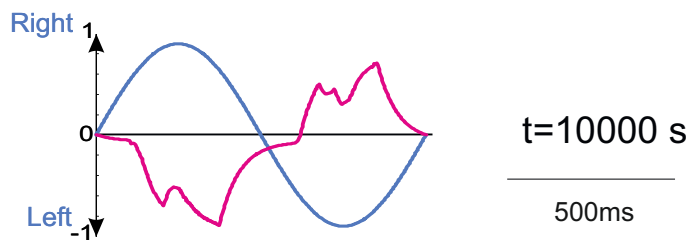


Figure S5-1

CS Purkinje Cell

no-CS Purkinje Cell

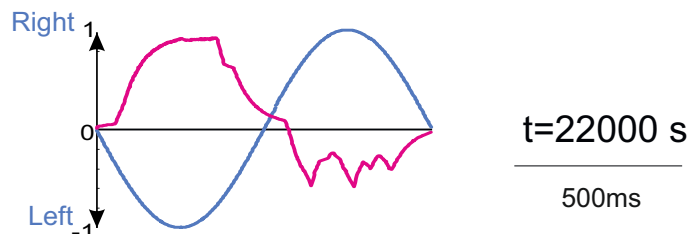
A



$t = 10000$  s

500ms

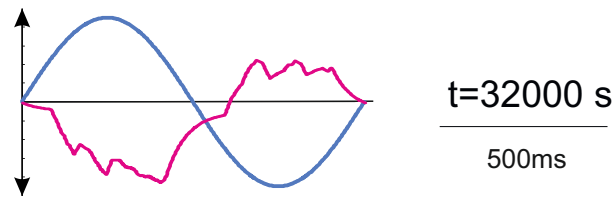
B



$t = 22000$  s

500ms

C



$t = 32000$  s

500ms

Figure S6-1

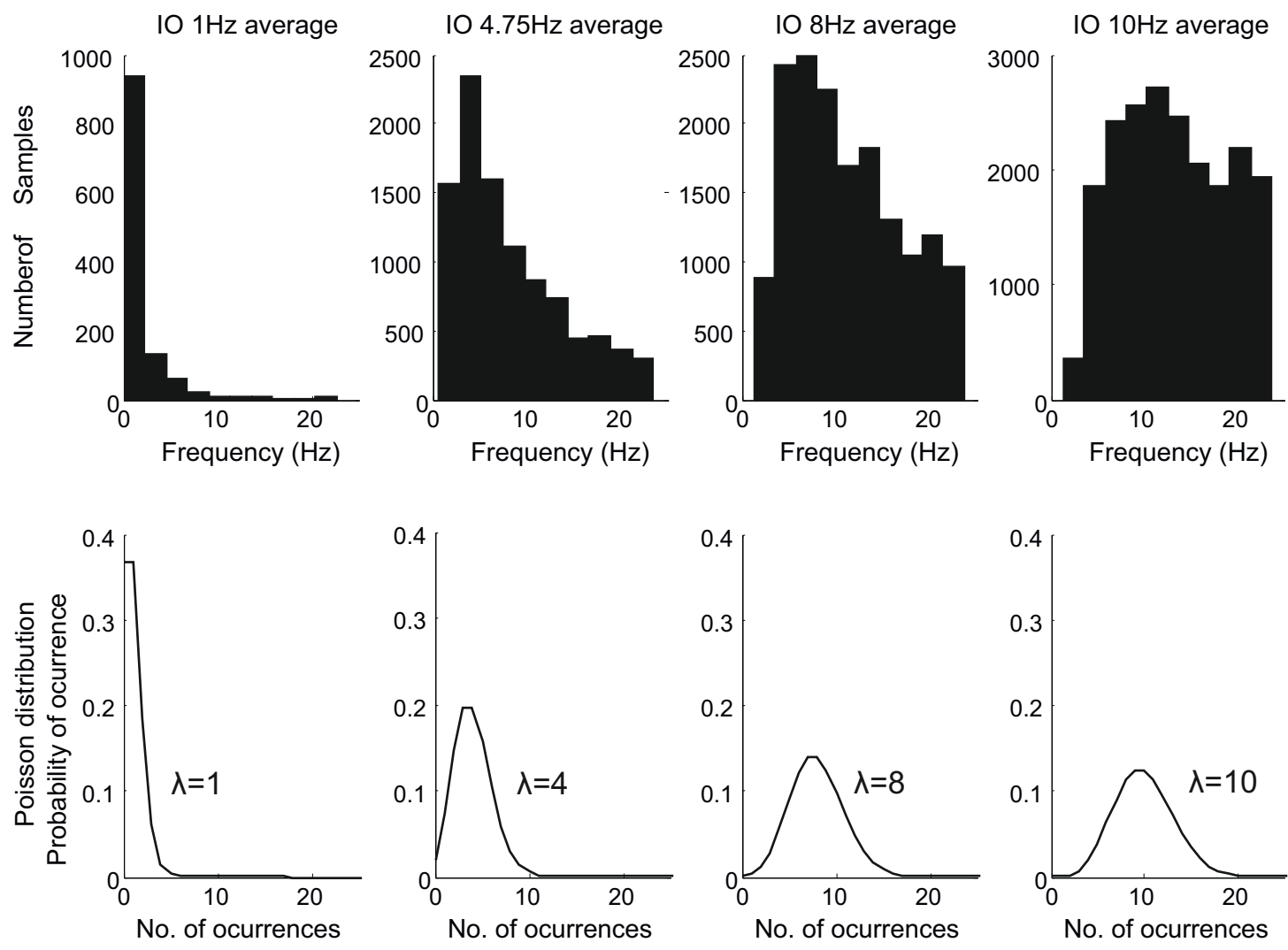


Figure S7-1